

Spring 2018

## Population Density and Spatial Distribution of Abyssal Epibenthic Holothurians Using Fine Scale Time Series Imagery (2007-2017)

Larissa Lemon

California State University, Monterey Bay, llemon@csumb.edu

Follow this and additional works at: [https://digitalcommons.csumb.edu/sns\\_theses](https://digitalcommons.csumb.edu/sns_theses)

---

### Recommended Citation

Lemon, Larissa, "Population Density and Spatial Distribution of Abyssal Epibenthic Holothurians Using Fine Scale Time Series Imagery (2007-2017)" (2018). *SNS Master's Theses*. 38.  
[https://digitalcommons.csumb.edu/sns\\_theses/38](https://digitalcommons.csumb.edu/sns_theses/38)

This Master's Thesis (Open Access) is brought to you for free and open access by the School of Natural Sciences at Digital Commons @ CSUMB. It has been accepted for inclusion in SNS Master's Theses by an authorized administrator of Digital Commons @ CSUMB. For more information, please contact [digitalcommons@csumb.edu](mailto:digitalcommons@csumb.edu).

POPULATION DENSITY AND SPATIAL DISTRIBUTION OF ABYSSAL  
EPIBENTHIC HOLOTHURIANS USING FINE SCALE  
TIME SERIES IMAGERY (2007-2017)

---

A Thesis  
Presented to the  
Faculty of the  
School of Natural Sciences  
California State University Monterey Bay

---

In Partial Fulfillment  
of the Requirements for the Degree  
Master of Science  
in  
Applied Marine and Watershed Science

---

by  
Larissa Lemon  
Spring 2018

**CALIFORNIA STATE UNIVERSITY MONTEREY BAY**

The Undersigned Faculty Committee Approves the

Thesis of Larissa Lemon:

**POPULATION DENSITY AND SPATIAL DISTRIBUTION OF ABYSSAL  
EPIBENTHIC HOLOTHURIANS USING FINE SCALE  
TIME SERIES IMAGERY (2007-2017)**



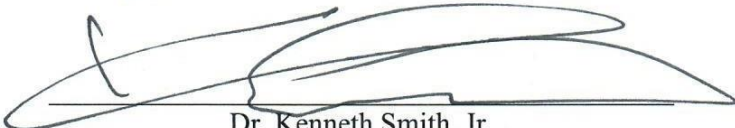
---

Dr. James Lindholm  
School of Natural Sciences



---

Dr. Alison Haupt  
School of Natural Sciences



---

Dr. Kenneth Smith, Jr.  
Monterey Bay Aquarium Research Institute



---

Dr. Christine Huffard  
Monterey Bay Aquarium Research Institute

---

Kris Roney, Dean  
Associate VP for Academic Programs and Dean of Undergraduate and Graduate Studies

---

Approval Date

Copyright © 2018

by

Larissa Lemon

All Rights Reserved

## ABSTRACT

Population density and spatial distribution of abyssal epibenthic holothurians using fine scale time series imagery (2007-2017)

by

Larissa Lemon

Master of Science in Applied Marine and Watershed Science  
California State University Monterey Bay, 2018

Holothurians are one of the most abundant megafauna observed in abyssal deep-sea communities and are important in the distribution of nutrients in the deep-sea. Despite their abundance and importance, there is little known about their natural history and population dynamics. These taxa respond to fluctuations in organic carbon supply, which originates as surface primary production and sinks through the water column. Previous studies have estimated population density and spatial ecology based on seasonal or monthly observations, that cannot detect fine-scale temporal changes. This study examines the rapid changes in population of 16 holothurian species observed at Station M, a long-term time series site Station M in the northeast Pacific, over a ten year period (2007 - 2017) using hourly time-lapse imagery and periodic videographic surveys conducted with a remotely operated vehicle (ROV). Holothurian density, mainly driven by the dominance of *Peniagone* sp. A, peaked from November 2013 to January 2014. Lags between changes in mass flux and rapid holothurian community responses were recorded, with *Peniagone* sp. A and *Peniagone vitrea* showing the strongest correlation to *in situ* measured mass flux ( $r = 0.40$ ,  $p=0.015$ ;  $r=0.41$ ,  $p<0.0001$ ) with a lag of 149 and 100 weeks, respectively. Spatial distribution of holothurians did not differ with changes in density. Similar population density and spatial distances of holothurians were found in continuous time-lapse and seasonal ROV imagery. The results demonstrate the advantage of using high temporal resolution imagery with long-term presence on the sea floor coupled with periodic videographic surveys to characterize the ecology of deep-sea benthic communities. These foundational community and population data will be vital in quantifying any future changes associated with climate change and increased extractive activities on the seafloor.

## TABLE OF CONTENTS

	PAGE
ABSTRACT.....	iv
LIST OF TABLES.....	vii
LIST OF FIGURES .....	viii-ix
ACKNOWLEDGEMENTS.....	x
CHAPTER	
1 POPULATION DENSITY AND SPATIAL DISTRIBUTION OF ABYSSAL HOLOTHURIANS .....	11
Introduction.....	11
Methods.....	14
Study area.....	14
Field collection of camera tripod imagery .....	15
Field collection of remotely operated vehicle (rov) imagery.....	16
Field collection of mass flux carbon data .....	17
Data extraction from imagery: Population density .....	17
Data extraction from imagery: Spatial distances .....	17
Cross correlation analysis .....	18
Nearest neighbor indices.....	19
Results.....	20
Population density.....	20
Cross correlation analysis .....	24
Spatial distances.....	25
Discussion.....	29
Conclusion .....	33
2 BROADER IMPLICATIONS OF DEEP-SEA RESEARCH .....	35
REFERENCES .....	38
A SUPPLEMENTAL POPULATION DENSITY GRAPHS BY SPECIES .....	47
B SUPPLEMENTAL CROSS CORRELATION GRAPHS.....	62

C SPECIES COMPARISON BETWEEN CAMERA TRIPOD AND ROV  
TRANSECTS.....69

D R CODE .....70

## LIST OF TABLES

	PAGE
Table 1. Time lapse and ROV deployment dates and duration of observations (days).....	16
Table 2. Observed holothurian species list .....	21
Table 3. Holothurians observed in the time-lapse imagery .....	22
Table 4. Cross correlation of holothurian small scale density and mass flux at Station M.....	24
Table 5. Spatial pattern and nearest neighbor indices for ROV and Time-lapse imagery .....	28
Table 6. Nearest neighbor distance summary statistics and Mann-Whitney-Wilcoxon results.....	28
<b>Appendix A</b>	
Table A- 1. Mean population density for each species by deployment .....	61
<b>Appendix C</b>	
Table C-1. Species composition of holothurians in camera tripod and ROV imagery used in spatial distance analysis.....	69

## LIST OF FIGURES

	PAGE
Figure 1. Map of study area at Station M. ....	15
Figure 2. Weekly holothurian population density and mean mass flux for 2007-2017. .....	23
Figure 3. Box plots of population density designated by deployment.....	25
Figure 4. Relative distribution of holothurians in "high," "medium," and "low" density ROV transects.....	26

### Appendix A

Figure A-1. Weekly population density of <i>Peniagone</i> sp. A.....	47
Figure A-2. Weekly population density of <i>Scotoplanes globosa</i> .....	48
Figure A-3. Weekly population density of <i>Peniagone vitrea</i> .....	49
Figure A-5. Weekly population density of <i>Abyssoecumis abyssorum</i> .....	51
Figure A-6. Weekly population density of <i>Elpidia</i> sp. A .....	52
Figure A-7. Weekly population density of <i>Oneirophanta mutabilis</i> .....	53
Figure A-8. Weekly population density of <i>Pseudostichopus mollis</i> .....	54
Figure A-9. Weekly population density of <i>Paelopatides confundens</i> .....	55
Figure A-10. Weekly population density of <i>Peniagone papillata</i> .....	56
Figure A-11. Weekly population density of <i>Peniagone</i> sp. 1.....	57
Figure A-12. Weekly population density of <i>Peniagone</i> sp. 2 .....	58
Figure A-13. Weekly population density of Holothuroidea sp. 4.....	59
Figure A-14. Weekly population density of <i>Psychropotes</i> spp. ....	60
Table A- 1. Mean population density for each species by deployment. ....	61

### Appendix B

Figure B-1. Cross correlation results for total holothurians. ....	62
Figure B-2. Cross correlation results for <i>Peniagone</i> sp. A.....	63
Figure B-3. Cross correlation results for <i>Scotoplanes globosa</i> .....	64
Figure B-4. Cross correlation results for <i>Peniagone vitrea</i> .....	65

Figure B-5. Cross correlation results for Synallactidae gen sp.....	66
Figure B-6. Cross correlation results for <i>Abyssocucumis abyssorum</i> .....	67
Figure B-7. Cross correlation results for <i>Elpidia</i> sp.A. ....	68

## ACKNOWLEDGEMENTS

I would like thank my committee members for their support and guidance throughout my research. My committee advisor, Dr. James Lindholm's, mentorship during my years as both an undergraduate and graduate student is greatly appreciated. I would not be the scientist I am today without his advice and tutelage. I would like to thank Dr. Alison Haupt for keeping me grounded in reality and cheering me on through graduate school and motherhood alike. To Dr. Ken Smith, thank you for taking a chance on a summer intern and letting me build upon a summer project, turning it into a thesis. I have appreciated the chance to work with you at the Monterey Bay Aquarium Research Institute (MBARI). Dr. Christine Huffard- thank you for always pushing me to be a better, more robust researcher. I do not believe that I would be here without her continuous support. Lastly, I would like to thank Linda Kuhnz who set me on the path of researching deep-sea cucumbers in the fastest ten-week internship one can imagine. I hope we can work together again in the future.

I would like to thank everyone at MBARI. I have met some amazing people who are always willing to share their knowledge on any topic. Anyone would be lucky to work for such a discovery oriented workplace.

Also, I would be remiss if I didn't thank everyone at the Institute for Applied Marine Ecology (IfAME). Although my research for this thesis was not through IfAME, my foundational knowledge of research was learned during my time at IfAME working on trawl studies.

Finally, I would like to thank my friends and family for supporting me through all my research. My husband, Adam, has always supported my passion for research--even if he did not always understand what I was doing or why I would get so excited about creatures that are so ugly they are cute. I could not have done this without your love and support. Thank you for everything. Lastly, although he is too young to know it, my son Logan has been a driving force to continue my research so I can provide him a good future. One day he will know how hard I worked for this.

# CHAPTER 1

## POPULATION DENSITY AND SPATIAL DISTRIBUTION OF ABYSSAL HOLOTHURIANS

### INTRODUCTION

The vast expanse of the deep-sea has largely been unexplored, spatially and temporally. However, there are some notable deep-sea locations worldwide that have been examined over long periods of time (Smith et al. 2017, Billet et al. 2001). For instance, there have been significant changes found in both density and species dominance among holothurians in two long time-series abyssal sites in the Northeast Atlantic (Porcupine Abyssal Plain, or PAP), and the Northeast Pacific (Sta. M) (Wigham et al. 2003; Ruhl 2007). In addition to population densities and dominance, data on the downward flux of particulate carbon onto the seafloor were also collected (Smith and Kaufmann 1999; Lampitt et al. 2001). The PAP site saw a large increase of the holothurian *Amperina rosea*, a species that had previously been rarely observed at the site (Billet et al. 2001). Analysis of specimens collected indicated that the holothurians were feeding on fresh detritus located on the seafloor (Iken et al. 2001). At Sta. M, long-term changes in population density and body size have been observed throughout the 29-year time series (Ruhl 2007; Huffard et al. 2016). These demographics appear to be related to the changes in flux of particulate organic carbon (POC) from the overlaying surface waters (Ruhl and Smith 2004). It has also been suggested that not only the variability of food supply, but also the quality of that food, has impacts on the persistent changes in deep sea communities (Kiriakoulakis et al. 2001). Obtaining knowledge of how these communities react in response to rapid changes in their environment will foster more accurate predictions relative to how deep-sea communities respond to new anthropogenic pressures facing the ocean such as climate change and resource extraction.

Holothurians are the most abundant mobile epibenthic megafauna found on the deep-sea floor (Ruhl 2007). In the context of deep sea ecology, epibenthic megafauna are defined as organisms in the deep that live on or just above the surface sediments of the sea floor and are able to be detected in photographic imagery  $\sim >1\text{cm}$  (Grassel et al. 1975;

Rex 1981). Due to their role in distributing carbon in deep-sea ecosystems, holothurian abundance and distribution can significantly impact the food availability (particulate organic carbon or POC flux) and energy flow for other benthic assemblages (Smith 1992; Lauerman et al. 1996; Costa et al. 2014). As described previously, holothurians have shown distinct responses to shifts in food supply and primary production (Johnson et al. 2007; Smith et al. 2009).

Recent surveys at Sta. M have suggested that deep-sea populations change more rapidly than an annual sampling rate would detect. Populations can respond to rapidly changing quantity and quality of food sources from the surface can occur in a matter of months rather than years (Smith et al. 2006; Ruhl 2007; Johnson et al. 2007; Huffard et al. 2016). Finer scale measurements (hourly, daily, or weekly) will be better able to detect the speed at which these populations can respond to changes in their environment, including large injections of food from surface waters into the ecosystem.

The characterization of these deep-sea communities has traditionally come from benthic trawl surveys and video transects (Billet et al. 2010, Ruhl 2007). However, these techniques often only explore abundances and distribution over short periods of time: often just once or twice a year, over a period of a few days. The large gaps in time and uneven sampling rates in seasonal sampling makes lag and correlation analysis and not possible. Also, trawl samples from the deep may not always have an accurate account of the number of individuals or even particular species due to evisceration from hauling gear up to the surface, leading researchers to use biomass as a proxy for density (Billet et al. 2010). The overall lack of knowledge of deep-sea communities makes even those measurements invaluable, but having accurate density and identification may lead to better predictions of how communities are changing.

Previous studies at Sta. M have observed the community structure, abundance, and distribution of organisms using seasonal remotely operated vehicles (ROV) and camera sled videographic transects (Lauerman et al. 1996; Ruhl 2007; Kuhnz et al. 2014; Huffard et al. 2016). This site is unique in that it also has a long data set of carbon influx to the seafloor as well as corresponding time-lapse imagery dating back to 1989. While the detailed carbon flux data have been utilized in previous analyses of population response with videographic transects, the time-lapse imagery itself has not been used to

determine population densities. The combination of these data sets will allow for stronger analysis of correlations between populations and environmental factors. Previously, it has been assumed that despite short term seasonal changes, benthic populations remain essentially unchanged over periods of decades, and perhaps longer (Billet et al. 2001), but long time series data may allow detection of potential true decadal shifts should they exist in populations.

The amount of nutrients reaching the sea floor has increased at Sta. M in recent years (Smith et al. 2013; Huffard et al. 2016). With the increase to the food supply, there has been an overall increase in holothurian densities observed in seasonal ROV transects (Huffard et al. 2016). Due to the known links between holothurian populations and food supply (particulate carbon), the present study sought to detect rapid changes in the deep-sea community using hourly time-lapse imagery over the last 10 years (2007-2017). It was hypothesized that the recent influx of carbon would produce a bimodal response, an initial behavioral response to the influx, and a later reproductive response as the species are able to utilize the nutrients for growth and reproduction.

With the availability of the fine-scale resolution time-lapse imagery, I compared the spatial patterns of holothurian populations to determine if distribution changed in varying levels of density. Spatial patterns of individual organisms were measured using nearest neighbor distance as an indication of distribution (Clark and Evans 1954; Altman 1992; Boiman et al. 2008).

The primary questions addressed were: 1) How has the density of holothurian populations changed over a 10-year time series (2007-2017) using fine scale hourly time-lapse imagery? 2) What, if any, relationships do the holothurian species have to the mass flux of particulate carbon reaching the seafloor? 3) Does the organismal density influence the spatial distribution of holothurians? 4) Are there differences in holothurian species density and distribution between continuous time-lapse imagery and seasonal ROV imagery? Hypotheses were generated to reflect these larger questions.

Specific hypotheses tested:

1. Holothurian species density changed over time, with increases occurring after large inputs of carbon.

2. Individual species would demonstrate positive cross correlation with a lag from mass flux.
3. Density influences the distribution categorization (clustered, random, or dispersed) of holothurians on the sea floor.
4. There are differences at the same station over the same period of time between continuous time-lapse imagery and seasonal ROV transect imagery.

## **METHODS**

### **STUDY AREA**

This study was conducted using imagery from a long time-series abyssal site (Sta. M: 34° 50'N, 123° 00'W; ~4000 m depth) in the northeast Pacific Ocean maintained by the Monterey Bay Aquarium Research Institute. Biological and oceanographic data have been monitored at this site consistently since 1989. Sta. M is characterized by silty-clay sediments and low topographic relief (Smith et al. 1993, Smith et al. 1994). The majority Station M epibenthic megafauna observed are echinoderms, xenophyophores, and sponges (Kuhn et al. 2014). In 2009, Station M community structure shifted from a sessile sponge-dominated community to a holothurian-dominated community (Kuhn et al. 2014). Previous studies at this site have shown holothurians to represent 73% to 99% of the megafauna observed (Ruhl 2007; Kuhn et al. 2014). Moored sediment traps collected sinking particulate matter to estimate the amount of food reaching the sea floor from the surface with 10-day resolution (Smith et al. 1994; Smith and Druffel 1998; Ruhl and Smith 2004). A time-lapse camera monitored fine-scale changes in seafloor conditions and megafauna (at the base of the sediment trap mooring).

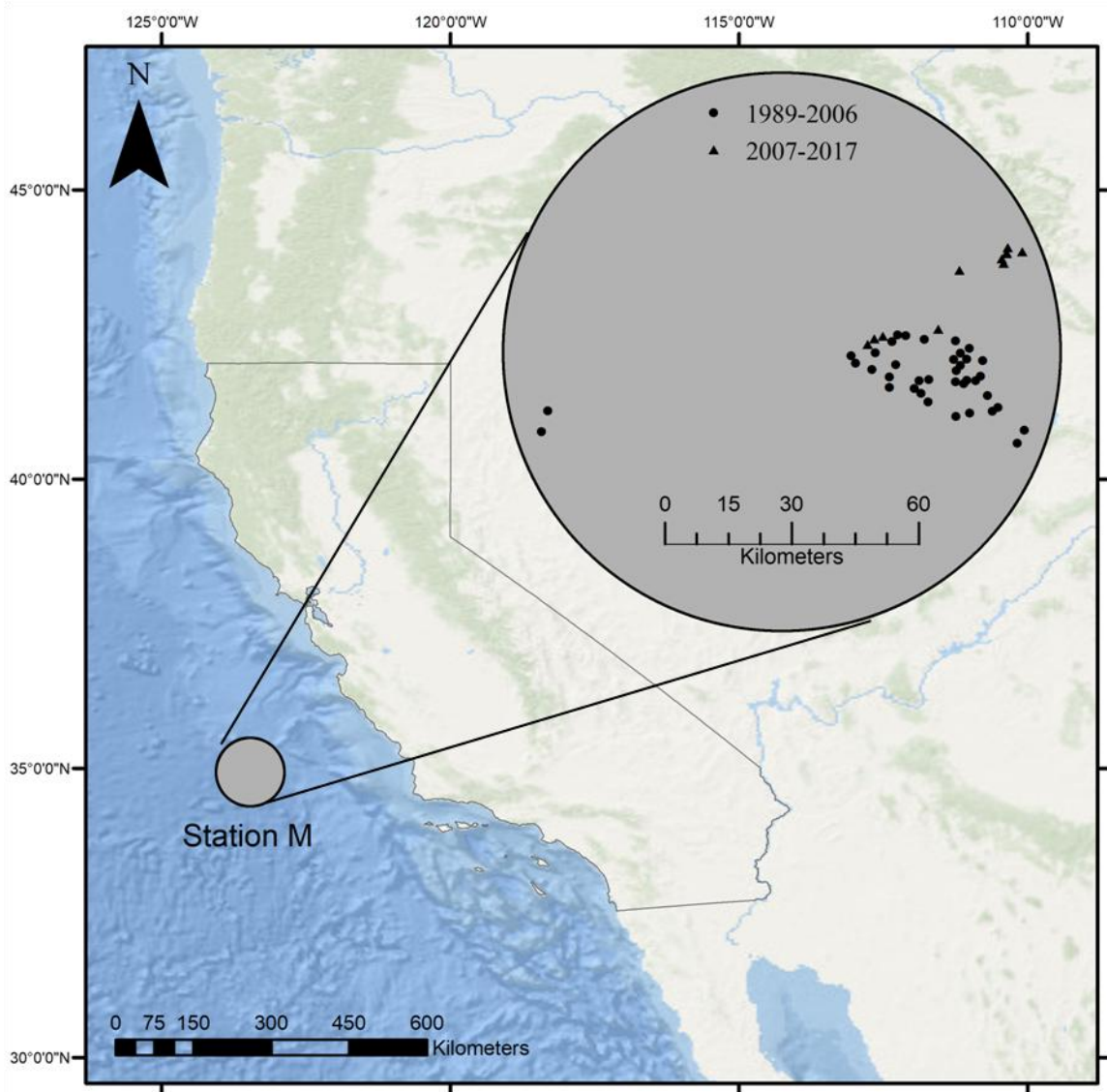


**Figure 1.** Map of study area at Station M. All points designate individual time lapse deployments (1989 to 2017). Triangles represent those deployments from 2007 to 2017 examined in this study.

### TIME-LAPSE CAMERA IMAGERY

The time lapse camera was deployed for long periods (up to a year at a time) since 1989. Mounted on a titanium frame at an angle of  $31^\circ$  in the horizontal plane and  $35^\circ$  in the vertical plane, the camera takes one still image of the seafloor every hour for the length of deployment. (Smith et al. 1993; Sherman and Smith 2009). The camera sits on the frame so the lens is approximately 2 m above the seafloor. Two strobes are mounted on either side of the camera housing to illuminate approximately  $20 \text{ m}^2$  of the seafloor.

The field of view begins at 1.8 m in front of the camera and extends to 6.5 m from the base of the tripod frame. The deployments in this study used high-resolution (3 x 5 mm) digital imagery.

#### REMOTELY OPERATED VEHICLE IMAGERY

ROV surveys were conducted coincident in time (2007 - 2017, Table 1) with autonomous mooring deployments at Sta. M. The ROV *Doc Ricketts* was equipped with Ikegama high-definition cameras with HA10Xt.2 Fujinon lenses to capture forward-oblique imagery for use in transects. Six 17,000 Lumen LED lights in addition to four 250 watt incandescent lights provided consistent illumination of the seafloor. Paired lasers spaced 29 cm apart served as reference points within the area imaged to determine the field of view for the transect. The ROV was flown at a mean altitude of 1.5 meters above the substrate. Cameras were adjusted to have an approximate field of view of one meter wide, and approximately 2.7 m ahead of the ROV. The ROV flew at a targeted speed of  $0.1 \text{ m s}^{-1}$ .

**Table 1.** Time lapse and ROV deployment dates and duration of observations (days).

Deployment ID	Deployed Date	Recovery Date	# Days	Corresponding ROV Date
52	6/6/2007	9/19/2007	103	6/7/2007
53				9/21/2007
54				2/25/2009
55	11/4/2009	5/12/2010	188	
56	5/14/2010	11/6/2010	172	
57	11/7/2010	5/23/2011	196	5/24/2011
58	5/24/2011	11/18/2011	174	11/17/2011
59	11/20/2011	6/12/2012	202	6/12/2012
60	6/13/2012	11/15/2012	152	11/16/2012
61				6/17/2013
62	6/16/2013	4/5/2014	289	4/5/2014
63	4/7/2014	10/13/2014	186	10/13/2014
64	10/14/2014	6/21/2015	247	6/18/2015
65	6/22/2015	11/7/2015	135	11/7/2015
66	11/8/2015	6/14/2016	216	11/11/2016
67	11/9/2016	3/24/2017	135	3/25/2017
68	3/24/2017	11/14/2017	230	11/13/2017

## **MASS FLUX**

The amount of particulate matter sinking to the seafloor from surface waters is called mass flux. Data on particle flux were collected using sediment traps moored at 50 m and 600 m above the seafloor with a sampling resolution of 10 - 17 days (Baldwin et al. 1998). Particulate matter was collected in plastic collection cups and examined immediately after recovery when zooplanktonic swimmers were removed from the sample.

Samples were thawed and processed in the lab using methods described in Baldwin et al. (1998). Samples were freeze-dried, weighed and analyzed for total particulate mass ( $\text{mg}/\text{m}^2/\text{day}$ ). The samples were then corrected for salt content using  $\text{AgNO}_3$  titration (Strickland and Parsons 1972).

## **DATA EXTRACTION FROM IMAGERY: POPULATION DENSITY**

MBARI's open source Video Annotation Reference System (VARS) was used to make annotations to both video and still imagery (Schlining and Stout 2006). The software allows measurements of animals, area, and length to be made that take into account the tilt and height of the camera. To ensure confidence in the identification of animals to species level, the lower half of the frame was used to calculate population density because lighting levels were more consistent in this area ( $5.75\text{m}^2$ ). The holothurian abundance in this area was recorded once per day of deployment throughout the ten-year time period assessed in this study. The same hour (12:00) was used for all annotations to limit the influence of any diurnal patterns that may exist. If the images began after the pre-determined time, the closest timecode was used for that day's measurement. Likewise, the same method was used for days that ended before the 1200 time. These values were compared qualitatively to population density measures from ROV transects in Sta. M publications (Kuhnz et al. 2014). All density measures were given in number of individuals per  $\text{m}^2$ .

## **DATA EXTRACTION FROM IMAGERY: SPATIAL PATTERNS**

Using the population density means from each time-lapse camera deployment and a list of available ROV transects, three significantly different deployments were selected to determine the spatial distributions of holothurians in relation to small-scale

density (high, medium, and low). The distances between individuals in images were measured using the distance tool in VARS, which accounts for the oblique angle of the camera. The area used for spatial distance measurements in the time-lapse imagery was expanded due to a larger illuminated area the three particular deployments selected, allowing for 75% of the total image to be used (16.1975 m<sup>2</sup>). Within each deployment's image series, 400 randomly selected frames were used to measure the distances between individuals. Time-lapse frames that fell within one week after the transect date were used for comparison to the ROV transect imagery.

For the ROV transects corresponding to the time-lapse camera deployment date, a subsample of 200 m was taken for distance analysis. The width of the frame as well as the coordinates of each holothurian within the frame were recorded in VARS. This approach allowed for the relative location of each individual along the transect to be annotated. Although geographic latitude and longitude coordinates were obtained, the resolution of the distances between these organisms (millimeters) was smaller than the resolution of the navigation data (meters), thus relative location along the transect was used for analysis (Norcross and Meuter 1999). Compilation of the coordinates by time (milliseconds) via the timecode recorded on the ROV was used to show relative distribution of holothurians in the ROV transects.

### **CROSS CORRELATION ANALYSIS**

Cross correlation functions were applied using the ranked population density and mass flux data. Calculations were conducted using R Statistical Software (R Core Team 2013; R Studio 2015; package = `ccf( )`) to identify (in terms of lag) the first positive correlation peak, as well as, the highest cross correlation peak up to a maximum lag of 260 weeks (R codes in Appendix D). This maximum lag (260 weeks or 5 years) was chosen based on limited research of various shallow-water holothurian species living 4 to 12 years (Ebert 1978; Michio et al. 2003).

Cross correlation analysis was limited to six individual species that had at least one percent of the observations made from the time-lapse imagery. Analysis was also done on the total holothurian population density. Shapiro-Wilk test (package = `shapiro.test( )`) was used to determine if the data were normally distributed. The data were transformed into ranks to account after the data was found to not be normally

distributed. Results from the cross correlation were used to identify the lag time at which initial and maximum peaks of positive correlation occurred between population density and mass flux (Appendix B). Once the lags of the data were determined for each species, effective sample sizes ( $N^*$ ), corrected correlation coefficients ( $r$ ) and p-values were calculated using methods addressing effective sample sizes and autocorrelation described in Pyper and Peterman (1998).

#### NEAREST NEIGHBOR INDICES

Using the previously described spatial data collected in both time-lapse and ROV imagery, the nearest neighbor distances were calculated into the nearest neighbor index (NNI). This measurement allows for the calculation of the mean nearest neighbor ratio:

$$NNI = \frac{\bar{D}_{observed}}{\bar{D}_{expected}}$$

where  $D_{observed}$  is the observed mean distance between each organism and its nearest neighbor:

$$D_{observed} = \frac{\sum_{i=1}^n d_i}{n}$$

and  $D_{expected}$  is the expected mean distance for a given a random distribution pattern:

$$D_{expected} = \frac{0.5}{\sqrt{\frac{n}{Area}}}$$

The  $d_i$  is the distance between each individual ( $i$ ) and its nearest neighbor while the  $n$  corresponds to the total number of individuals. The area corresponds to the total area surveyed. Categorizations of distribution (clustered, random, or dispersed) are assigned based on the calculations. Subsequent z-scores (standard normal variate) are also

calculated to assess 95% confidence intervals of the NNI being the correct categorization. A negative z-score indicates clustering while a positive score indicates dispersion or evenness (Boots et al. 1988).

$$z = \frac{\bar{D}_{observed} - \bar{D}_{expected}}{SE}$$

Lastly, a Mann Whitney U test was conducted to see if there were differences between the nearest neighbor distances observed in the ROV and time-lapse imagery. Summary statistics and Mann Whitney calculations were conducted using R Statistical Software (R Core Team 2013; R Studio 2015; package = wilcox.test( )).

## RESULTS

### POPULATION DENSITY

This study examined approximately 280 m<sup>2</sup> of seafloor from 2007 to 2017 using time-lapse images. Population density was annotated for 2623 days. Overall, 8296 individual holothurians representing 16 species (Table 2) were observed in the time-lapse imagery. Due to difficulties in confidently distinguishing between some small *Peniagone* species, indistinguishable individuals were binned together into a group called *Peniagone* for analysis. Also, *Psychropotes depressa* and *Psychropotes longicauda* were observed in such low numbers that observations were combined into a *Psychropotes* spp. category for analysis.

Three species accounted for over 91% of the observations made in the time-lapse imagery: *Peniagone* sp. A (72.13%; 5984 individuals); *Scotoplanes globosa* (16.51%; 1370 individuals); and *Peniagone vitrea* (2.63%; 218 individuals). Number of individuals and percentages of the observations can be seen in Table 3.

**Table 2.** Observed holothurian species list. Asterisk (\*) indicates species that have been identified as undescribed, but not yet named.

<b>Species List</b>	
<b>Class Holothuroidea</b>	Holothuroidea sp. 4*
<b>Order Aspidochirotida</b>	
Family Synallactidae	<i>Paelopatides confundens</i> <i>Pseudostichopus mollis</i> <i>Synallactidae</i> gen.*
<b>Order Dendrochirotida</b>	
Family Cucumariidae	<i>Abyssocucumis abyssorum</i>
<b>Order Elasipodida</b>	
Family Deimatidae	<i>Oneirophanta mutabilis</i>
Family Elpidiidae	<i>Elpidia</i> sp. A* <i>Peniagone gracilis</i> <i>Peniagone papillata</i> <i>Peniagone</i> sp. 1* <i>Peniagone</i> sp. 2* <i>Peniagone</i> sp. A* <i>Peniagone vitrea</i> <i>Scotoplanes globosa</i>
Family Psychropotidae	<i>Psychropotes depressa</i> <i>Psychropotes longicauda</i>

**Table 3.** Holothurians observed in the time-lapse imagery. Species that had at least one percent of the observations were used in the cross correlation analysis.

Species	# Individuals Observed	% Observations
<i>Peniagone</i> sp. A	5984	72.13%
<i>Scotoplanes globosa</i>	1370	16.51%
<i>Peniagone vitrea</i>	218	2.63%
Synallactidae gen.*	125	1.51%
<i>Abyssoicum abyssorum</i>	116	1.40%
<i>Peniagone</i> sp.	101	1.22%
<i>Elpidia</i> sp. A	100	1.21%
<i>Oneirophanta mutabilis</i>	52	0.63%
<i>Pseudostichopus mollis</i>	45	0.54%
<i>Paelopatides confundens</i>	44	0.53%
<i>Peniagone papillata</i>	41	0.49%
<i>Peniagone</i> sp. 1	29	0.35%
<i>Peniagone</i> sp. 2	29	0.35%
Holothuroidea sp. 4	25	0.30%
<i>Psychropotes</i> spp.	17	0.20%
<b>Total:</b>	<b>8296</b>	

The population densities of all holothurian species' were variable over the ten-year period studied here. The 10-year mean density of holothurians was 0.56 individuals/m<sup>2</sup>. The highest densities observed were between November 2013 ( $\bar{x} = 2.02$  individuals/m<sup>2</sup>) and December 2013 ( $\bar{x} = 2.00$  individuals/m<sup>2</sup>) (Figure 2A). The weekly density peaked at 2.36 individuals/m<sup>2</sup> in January 2014, attributable largely to the abundance of *P. sp. A*. There were also years that were characterized by low density. The lowest observed density occurred in June of 2007 ( $\bar{x} = 0.06$  individuals/m<sup>2</sup>) when no holothurians were observed for two consecutive weeks. Individual species density in comparison to the total holothurian density is detailed in Appendix A. The densities observed from previous ROV transects followed similar trend lines as the time-lapse imagery. However, four transects showed much higher density than time-lapse imagery.

Mean densities for each species and deployment provided information about how these populations shifted over time (Appendix A, Table A-1). Ten of the 15 species

categories had density peaks in a 2-year period between June 2012 and October 2014.

*Peniagone* sp. A was the most abundant species observed until November 2016 to November 2017 when *S. globosa* became more abundant.

The ten-year mean of the mass flux sinking to the seafloor was 135.49 mg/m<sup>2</sup>/day (Figure 2B). Mass flux was collected for 292 of the 383 weeks observed. The mass flux had multiple periods of time when detritus was higher than the ten-year average. The largest period of mass flux occurred in June 2011 ( $\bar{x} = 543.86$  mg/ m<sup>2</sup>/day), peaking at 770.61 mg/ m<sup>2</sup>/day for a single collection cup (10 days). The lowest periods of mass flux occurred between November 2015 and February 2016 with a range of 23.46 to 34.84 mg/ m<sup>2</sup>/day.

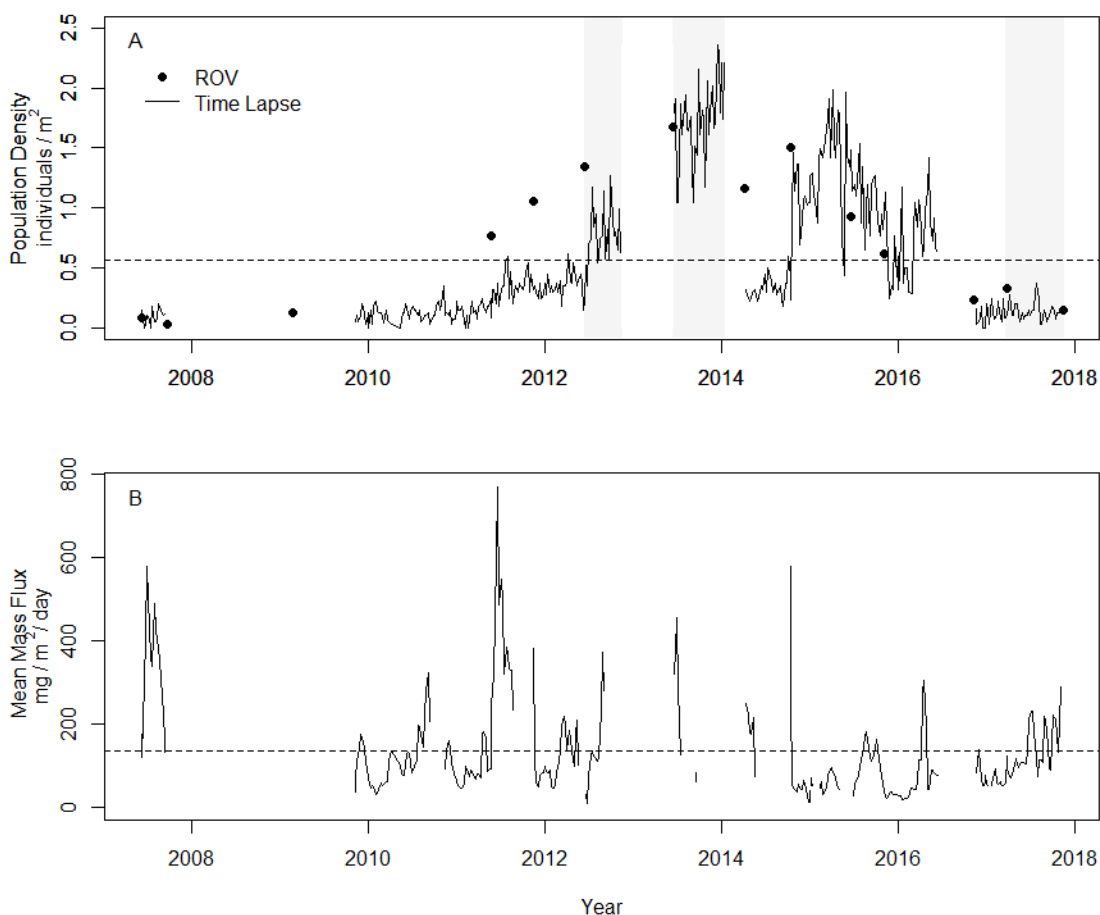


**Figure 2.** Weekly holothurian population density and mean mass flux for 2007-2017. ROV population density data are represented by points while the weekly density averages are denoted by the line. Gray areas denote deployments used for high (62), medium (60), and low (68) density spatial distribution analysis.

## CROSS CORRELATION ANALYSIS

The correlation describes the strength of the relationship of population density to mass flux. Although most of the species examined had a p-value significance coinciding with at least one peak, the correlation values were not strong (Table 4). For example, *Abyssocucumis abyssorum* showed a significant initial response to the mass flux reaching the seafloor with a lag of -48 weeks, the relationship was only 10% correlated ( $r=0.10$ ,  $p\text{-value} = 0.009$ ). *Peniagone* sp. A and *P. vitrea* had the strongest correlation with mass flux ( $r = 0.40$ ,  $p\text{-value} = 0.015$ ; and  $0.41$ ,  $p\text{-value} < 0.0001$  respectively) with lags of -103 and -100 weeks. *Scotoplanes globosa* was the only species without a significant correlation with mass flux.

**Table 4.** Cross correlation of holothurian small scale density and mass flux at Station M. Effective sample size (N\*), correlation coefficients (r), and p-values were corrected for autocorrelation according to Pypers and Peterson (1998).

Species	Peak	Lag (in weeks)	Sample Size (N)	Effective Sample Size (N*)	Correlation (r)	p-value
<i>Peniagone</i> sp. A	Initial	-103	364	33.1	0.33	0.057
	Max	-149	332	37.9	0.40	0.015*
<i>Scotoplanes globosa</i>	Initial	-176	293	37.6	0.12	0.471
	Max	-203	324	234.7	0.13	0.53
<i>Peniagone vitrea</i>	Initial	-57	352	103.1	0.21	0.034*
	Max	-100	382	103.9	0.41	0.00002***
<i>Synallactidae</i> sp.	Initial	-141	256	76.7	0.16	0.173
	Max	-210	313	111.5	0.28	0.003**
<i>Abyssocucumis abyssorum</i>	Initial	-48	338	156	0.10	0.009**
	Max	-146	303	144.7	0.22	0.207
<i>Elpidia</i> sp. A	Initial	-25	363	87.1	0.20	0.06
	Max	-82	376	85.4	0.23	0.033*
All Holothurians	Initial	-103	312	26.6	0.24	0.237
	Max	-149	322	35.2	0.4	0.017*

### SPATIAL DISTRIBUTIONS

The three significantly different deployments selected based on population density means and Kruskal-Wallis test ( $p$ -value  $< 0.0001$ ; Figure 3). The ROV transects were subsampled, accounting for a combined  $600 \text{ m}^2$  used for spatial distribution comparisons. There were 14 holothurian species and 815 individuals observed in the ROV transects. Relative locations of holothurians were plotted for each transect (Figure 4). The high density transect (ROV<sub>high</sub>) had 411 individuals, dominated by *Peniagone* sp. A (N=154) and *Elpidia* sp. A (N=132), and a substantial number of *Scotoplanes globosa* (N=75) (Fig. 4A). The medium density transect (ROV<sub>med</sub>) was also mostly comprised by *E. sp. A* (N=156) and *P. sp. A* (N=118) (Fig. 4B). Lastly, the low density transect (ROV<sub>low</sub>) observed 47 individuals observed. *Scotoplanes globosa* was the most abundant species (N=17) followed closely by *P. sp. A* (N=12) (Fig. 4C).

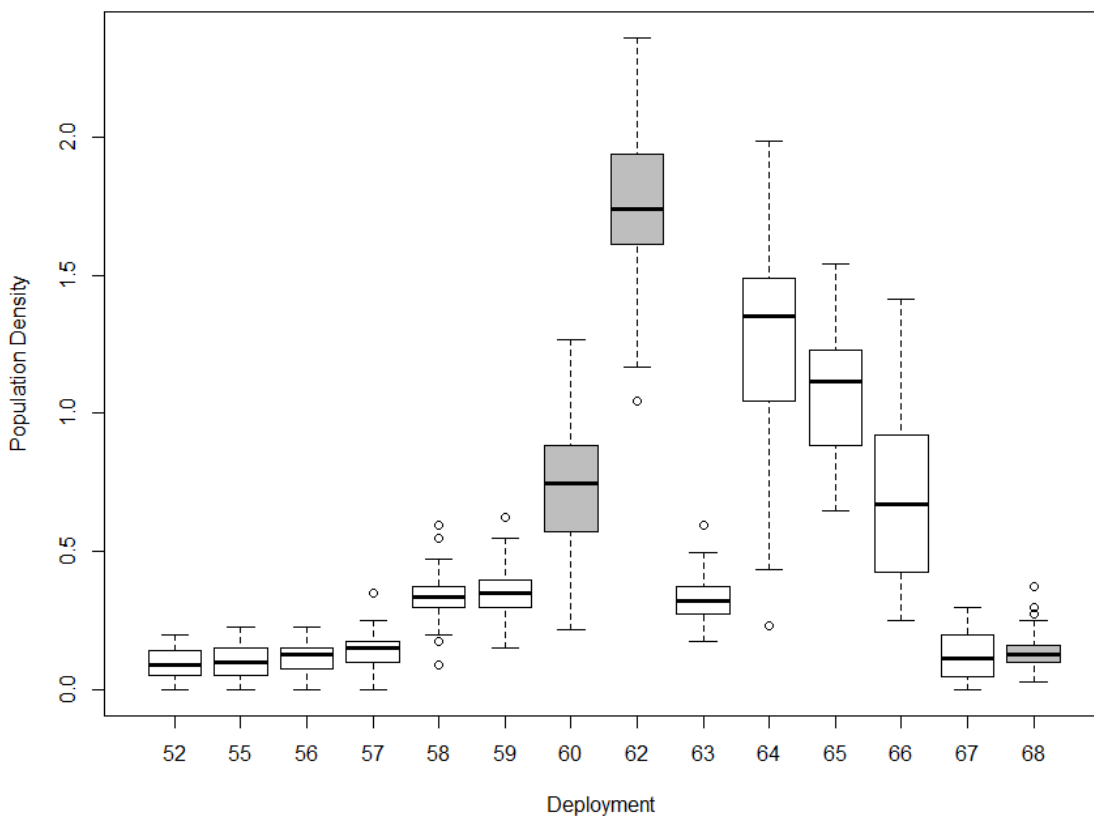


**Figure 3.** Box plots of population density designated by time lapse camera deployment. The gray deployments were those selected for spatial distance analysis: high density (62), medium density (60), and low density (68).

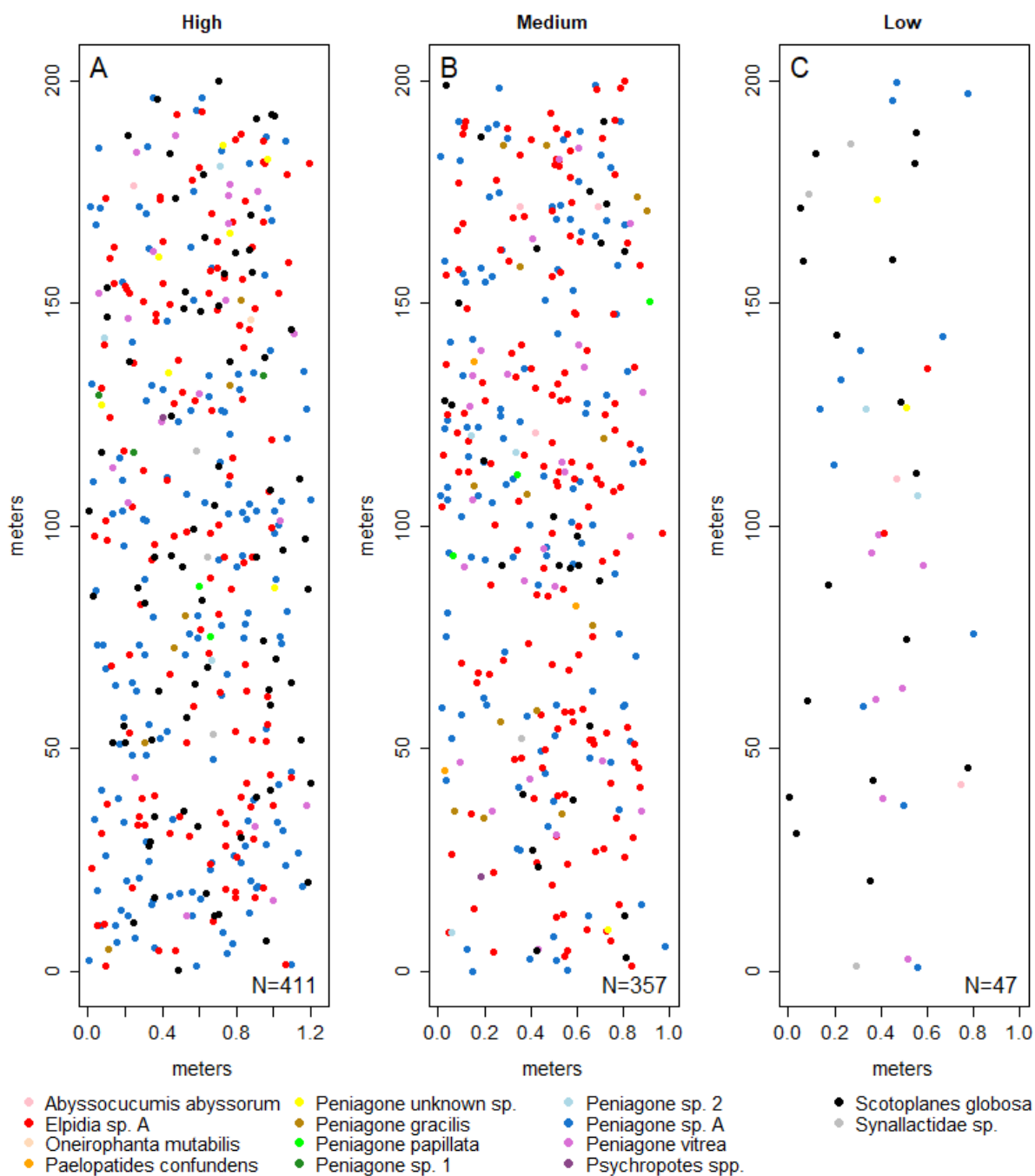


**Figure 4.** Relative distribution of holothurians in "high," "medium," and "low" density ROV transects. (A) coincides with time-lapse deployment in June 2013, representing high density (N=411); (B) corresponds to a deployment in June 2012, representing medium density of holothurians (N=357). (C) pairs with a deployment in November 2017 and is considered to be low density (N=47). Nearest Neighbor Index was calculated for all of these transects.

The time-lapse imagery showed 45 frames that fell within the one week time parameter of the ROV transects. The high density time period (TL<sub>high</sub>) had 24 frames, in which 270 individuals were observed. Although the top three species were the same as in the ROV<sub>high</sub> transect of, the proportion of individuals was different (*Peniagone*. sp. A=220; *Elpidia* sp. A=13; *Scotoplanes globosa* = 17). *Elpidia* sp. A was observed significantly less in the time-series images. Even taking into account the differences in sampling area, the density of the *E.* sp A was lower (0.08 individuals/m<sup>2</sup> compared to 0.78 individuals/m<sup>2</sup> in the ROV). Eleven frames were examined in the medium density time period (TL<sub>med</sub>). There were 25 individuals with all but three being *P.* sp. A and no *E.* sp. A observed, a change from the composition observed in the ROV<sub>med</sub> transect. The low density time-lapse imagery (TL<sub>low</sub>) used 10 frames, and found 14 individuals. *Scotopolanes globosa* was the dominant species (N=10). Full comparisons of species presence in all samples (time-lapse and ROV) used for spatial pattern analysis can be seen in Appendix C.

The nearest neighbor index for time-lapse and ROV imagery were similar. All time-lapse measurements resulted in a dispersed distribution patterns. Likewise, ROV nearest neighbor index calculations reflected the same, with one transect (ROV<sub>med</sub>) getting categorized as random rather than dispersed (Table 5). The mean nearest neighbor distances observed in the time-lapse were slightly farther in distance than those calculated with the ROV transects for all density categories. For example, in the high density ROV imagery, the average nearest neighbor distance was 0.40m ± 0.28. The same time period observed 0.71m ± 0.53 in the time-lapse imagery. The same was true in the medium and low density periods as well (TL<sub>med</sub>:  $\bar{x}$  = 1.07m ± 0.71; ROV<sub>med</sub>:  $\bar{x}$  = 0.41m ± 0.33 and TL<sub>low</sub>:  $\bar{x}$  = 2.73m ± 0.75; ROV<sub>low</sub>:  $\bar{x}$  = 1.83m ± 1.78, respectively). These nearest neighbor distances were significantly different in all density levels (Table 6).

**Table 5.** Spatial pattern and nearest neighbor indices for ROV and Time-lapse imagery.

	Method	Date(s)	# Samples	# Individuals	NNI	Z-score	Distribution
High Density	Time-lapse	6/16/2013 - 6/22/2013	24	270	1.234	4.595	dispersed
	ROV	6/16/2013	1	411	1.151	3.748	dispersed
Medium Density	Time-lapse	6/12/2012 - 6/19/2012	11	25	1.373	2.251	dispersed
	ROV	6/12/2012	1	356	0.407	1.880	random
Low Density	Time-lapse	11/10/2017- 11/17/2017	10	14	1.917	6.484	dispersed
	ROV	11/14/2017	1	47	1.771	3.067	dispersed

**Table 6.** Nearest neighbor distance summary statistics and Mann-Whitney-Wilcoxon results. Mean nearest neighbor distances and standard deviation (SD) shown. Mann-Whitney-Wilcoxon results show significant differences between measured NN distances in imagery methods

	Method	$\bar{x}$ NN Distances	SD	W	p-value
High Density	Time-lapse	0.71	0.53	1757	<0.00001***
	ROV	0.40	0.28		
Medium Density	Time-lapse	1.07	0.71	35274	<0.00001***
	ROV	0.41	0.33		
Low Density	Time-lapse	2.73	0.75	146	<0.0001**
	ROV	1.83	1.78		

## DISCUSSION

The composition and population density of the holothurian community in the deep-sea was shown to be variable over the ten-year period examined in this study. The progression of measurements over multiple deployments (13 in the ten-year period) at Station M suggests these data show a population response rather than an opportunistic response to patchy detritus. The dominance of deposit-feeding holothurians in the deep-sea epibenthic community is similar to the diverse assemblages of deposit-feeders found in shallow-water soft-bottomed habitats (Thrush 1991, Morrisey 1992; Kelaher and Levinton 2003). As in the shallow-water communities, the deep-sea community responds to changes in the amount of detritus reaching the seafloor (Rhoads et al. 1978; Thrush 1996; Ruhl and Smith 2004).

The observed holothurian density was relatively low from 2007 through 2011, before increasing. Although the population density increased after a large influx of nutrients in June 2011, there were other influxes that didn't appear to have the same response in the population growth. There is evidence that the quality of detritus is important to the response of holothurian species. *Abyssocucumis abyssorum* and *Scotoplanes globosa* selectively feed on fresh detritus whereas some *Elpidia* sp. are less selective in their feeding preferences (Lauerman et al. 1997; Miller et al. 2000; Jamieson et al. 2011). The breadth of this research on deep-sea holothurians compared to shallow-water species is limited due to difficulties in collecting and maintaining individuals in a controlled lab setting.

The increased population density was largely attributed to a single species, *Peniagone* sp A. There may be multiple factors that explain why this species responded to the June 2011 flux event. First, *Peniagone* sp A has been observed swimming (personal observation), suggesting immigration and recruitment to areas with the richest nutrients is possible (Gebruk 1995). Other species in the genus *Peniagone* have also been observed swimming in the water column (personal observations; Kaufman and Smith 1997; Ruhl 2007). Huffard et al. (2016) saw evidence of potential immigration and juvenile recruitment based on body length of holothurians at Station M within the time period of this study. Another possible factor of response could be their ability to detect the nutrients. There is some evidence of holothurians having a network of nerves and

sensory buds on the skin to detect chemical stimuli (Lambert 1997). *Holothuria forskali*, a shallow-water holothurian, has sensory organs on their buccal tentacles (feeding tentacles) to facilitate detection of rich sediment patches through the chemosensitive abilities of their apical buds (Massin 1982; Boulard et al 1982).

The rapid increase and subsequent decline of *Peniaogone* sp. A is a phenomenon that has been observed in other holothurian species (Bett et al. 2001; Billet et al. 2001; Smith et al. 2009). *Amperima rosea* and *Ellipinion molle* densities at the deep-sea site in the northeastern Atlantic (Porcupine Abyssal Plain, PAP) increased by orders of magnitude in an event that lasted approximately 3 years (Billet et al. 2001; Rodrigues et al. 2001). The rates of change for the holothurian density in this study varies from previous studies at this site (Huffard et al. 2016). It is hypothesized that this style of boom-bust population variation is part of the evolutionary life history characteristics of many echinoderms (Uthicke et al. 2009). Unfortunately, there is very little known about life history, fecundity and longevity of many of these deep-sea species due to difficulties in collecting intact specimens. It is difficult to predict how populations will respond to changes in their environment without knowing reproductive behaviors, maturity, and lifespan of these organisms.

There is additional evidence that suggest some species of epibenthic fauna, including holothurians, exhibit cyclical pattern in density on a decadal scale at Station M (Kuhnz et al. 2014). In previous studies looking at data from 1989 to 2012, *Elpidia* sp. A was the dominant organism in the community for a decade, yet became nearly undetectable for over a decade after that (Kuhnz et al. 2014). If this type of time cycle is happening, the importance of long-term time series data becomes an essential aspect of understanding deep-sea community structure and population dynamics.

#### **MECHANISMS FOR LAGGED RESPONSES TO MASS FLUX**

The recruitment, behavior, and migration of holothurians may have an important impact on the response time of a species to influx of nutrients onto the seafloor. *Elpidia* sp. A. had the fastest initial response to mass flux (25 weeks), followed by *Abyssocucumis abyssorum* (48 weeks). These two species exhibit a run and mill pattern of activity wherein they quickly move across large distances in a short amount of time (Kaufmann and Smith 1997). Then, they meander around a particular area for a prolonged

period of time at slower speeds (Kaufmann and Smith 1997; Jamieson et al. 2011). This patterned activity may allow them to find detritus on the seafloor quicker than other species, which is indicated by having the least amount of lag response to the mass flux. These species have also been observed burrowing into the sediment at Station M (Ken Smith, personal communication), which leads to other possibilities as to their relatively rapid response to mass flux. There is some evidence that holothurians are able to shift their diet based on availability of nutrients (Piersma and Dent 2003). By burrowing into the sediment, these holothurians may be able to opportunistically feed on other nutrient layers of detritus stratified within the sediment (Shirayama 1984). Lastly, there is evidence of holothurians entering into a dormancy state when subjected to environmental stressors, including low food supply (Cáceres 1997; Klanian 2013). If this is the case for *Elpidia* sp. A and *A. abyssorum* then they might remain buried and emerge to become more active once there is detection of an increased food supply.

*Peniagone vitrea* and *P. sp. A* showed the strongest correlation (0.41 and 0.40, respectively) to the mass flux. All known swimming holothurians are planktonic in nature, using currents to carry them long distances (Roberts et al. 2000; Rogacheva et al. 2012). The conditions of the deep-sea (generally low food supply punctuated by large episodic influxes and patchy distribution of those nutrients) force some deposit-feeders to adapt with a more mobile strategy of foraging (Rogacheva et al. 2012). However, they are able to control when they land on the seafloor by ingesting marine snow in the water column and collecting detritus just off the seafloor with their tentacles to use as ballast in their body (Pawson 1986; Miller & Pawson 1990). This behavior may allow these species to cover a large expanse of habitat, but not control the exact direction in which the holothurians are moving. Once these species sense the detritus, they might make an active decision to land. This could explain why it has a strong correlation to mass flux, but takes 100 to 150 weeks to find those nutrients.

#### **DENSITY AND COMPETITION**

Density did not appear to have an impact on the distribution of holothurians at Station M. The lack of influence of density on distribution suggests there is resource partitioning occurring among deep-sea holothurians, like that observed in tropical holothurians (Roberts 1979). The high diversity of holothurians in the deep sea may be

attributed to the wide variety of feeding and digestive strategies these species employ (Roberts et al. 2000). By having different feeding behaviors and tentacle morphology, the holothurians might not be consuming, and therefore competing for, the same particles of detritus reaching the seafloor.

Holothurians utilize tentacles to transfer food particles to their pharynx (Lawrence 1987; Roberts et al. 2000). There are five different morphological groups of tentacles in holothurians, but even tentacles of the same group may be used differently depending on the feeding behavior of the species (Massin 1982). Elapodidae (exclusively deep-sea holothurians) have three morphological tentacle types: peltate, digitate, and dendric (Hansen 1975; Gebruk 1995). Within those groups, there is further specialization of those tentacles based on branching structures and nodules (Bouland et al. 1982; Roberts et al. 2000). *Oneirophanta mutabilis* and *Psychropotes longicauda*, two species found at Station M, also have bacteria on their feeding tentacles that may break down detritus before ingestion (Moore 1994; Roberts et al. 2000). The utilization of these morphologies strategies allow for high diversity of holothurians in the deep-sea, without altering the distribution patterns observed.

#### **TECHNOLOGY COMPARISONS**

This study highlights differences in technologies used to study deep-sea megafauna, community composition, population density and movements (Smith et. al 1993; Billet et al. 2001; Ruhl 2007). There are inherent advantages and disadvantages to both the time-lapse camera tripod technology, seasonal ROV methods, and even trawl sampling.

Trawls have historically been quite useful in determining large-scale and long-term patterns of fish and invertebrate ecology (Billet et al. 2010). However, using trawls does not detect fine-scale spatial distribution of the organisms along the seafloor. This sampling method also tends to result in damaged specimens, which are difficult to identify and examine. Comparisons between time-lapse imagery and trawls indicates that trawls vastly underrepresent smaller individuals and species (Bett et al. 2001).

ROVs are able to sample relatively large areas, much like a trawl, but with capabilities to observe the exact distribution of megafauna. This technology requires personnel, ship time, and can be dependent upon environmental conditions that can limit

sampling periods. This makes rapid changes in communities difficult to detect. Also, there is some evidence that the operation of the ROV itself may impact the behavior of organisms, increasing the error of density measurements (Stoner et al. 2008).

The time-lapse camera provides details about the fine scale resolution of population shifts that cannot be detected in seasonal sampling. However, the larger field of view for the time-lapse camera may show bias against some species. For example, 156 *Elpidia* sp. A individuals were observed in a single ROV transect, yet the same time period in the time-lapse imagery only had 13 observations. The bias stems from the difficulty detecting the small, cryptic *Elpidia* in the time-lapse imagery. Previous studies have found *Elpidia* to range from 0.5 to 6.9 cm at Station M (Huffard et al. 2016). The time-lapse is only able to detect larger individuals. This may be true of other species, as well as juveniles of the holothurians we currently observe. Much like the ROV, the presence of a large piece of equipment on the deep-sea seafloor may create a reef effect much like oil platforms have shown to impact invertebrate assemblages in shallow-water environments (Page et al. 1999; Bram et al. 2005). Vardaro et al. 2007 addresses this concept with the time-lapse camera at Station M. They found no evidence that epibenthic megafauna was impacted by the equipment thus population data were not impacted by aggregation responses to the camera.

## CONCLUSIONS

The data examined here provides the first fine-scale resolution of the fluctuations in holothurian populations and movements. The deep-sea is often viewed as a stable, unchanging environment, but there can be rapid changes in populations due to outside environmental factors. Holothurian density has changed over the ten-year period from 2007 to 2017 with individual species showing more correlation with mass flux than others. Despite the differences in density, the spatial distribution patterns observed do not seem to change.

The influence of food supply is not the only potential force impacting deep -sea communities. There are external anthropogenic pressures that continue to face the oceans including resource extraction and climate change. More research is needed to determine how these populations and communities will react or adapt to those oncoming pressures.

The fine scale resolution of the time-lapse camera also gives researchers the ability to look into behaviors that holothurians exhibit in the deep-sea. In examining hourly images from Station M, I have observed both swimming and standing behaviors in holothurians. Although it may be difficult to attribute reasons for swimming, this dataset could indicate occurrences of swimming, adding to the natural history of these organism. Standing behaviors observed may provide important information on reproductive behaviors, a topic that is lacking for most deep-sea species. There may be more behaviors the time-lapse camera can detect to contribute to the limited knowledge of deep-sea communities.

## **CHAPTER 2**

### **BROADER IMPLICATIONS OF DEEP-SEA RESEARCH**

#### **RESOURCE EXTRACTION**

The mobile epibenthic megafauna, especially holothurians, are very important in the distribution of carbon and energy to many assemblages in the deep-sea (Smith 1993; Lauerman et al. 1996; Costa et al. 2014). The prevalence of this taxa across abyssal depths has made an indicator of how deep-sea communities change in response to changes in environment whether through food supply, physical disturbance or climate change (Thiel et al 1992; Bluhm et al. 1995; Ruhl and Smith 2004; Sweetman and Witte 2008; Smith et al. 2009). However, there are still large gaps in knowledge regarding population density, community structure, distribution, and life history of deep-sea organisms. The fine scale resolution of population dynamics is a step towards filling those gaps. This is becoming more important as technology and innovation drives humans to expand resource extraction to the deep-sea.

As coastal fisheries decline and technology improves, commercial fisheries are able to expand farther into deep waters (Koslow et al. 2000; Morato et al. 2006; Pitcher et al. 2010). Some estimates of global catch have estimated the catch of known deep water taxa to have increased six-fold over the last 50 years, with no sign of stopping (FAO 2017). In recent years, these increases have been facilitated by better and more accurate equipment (Pauly et al. 2003). Unfortunately, many deep-sea fish have less resilience than shallow-water and coastal counterparts (Baker et al. 2009). In addition to impacting fish populations, these fisheries are having an impact on the benthic community due to contact from trawl and long-line gears (Auster et al. 1999; Clark et al. 2016).

Another resource the deep-sea has long shown potential for is the mining of manganese nodules, manganese crust, and poly-metallic sulphides (Boschen et al. 2016; Scott 2001). Previous, failed attempts at these mining operations in the 1970s and 1980s put a halt to the active pursuit of mining in deep-sea basins (Scott 2001). The advent of new technologies and high prices of metals has led to resurgence by the mining industry to exploit these resources (Halfar and Fujita 2007). While the extraction of these minerals is not economically viable at present, many nations are depending on their

potential value in the future. Since most of these operations are outside exclusive economic zones, and internal body set up by the United Nations, the International Seabed Authority (ISA), has been given the task of regulating exploration and exploitation of non-living resources in international waters (Lodge et al. 2014). Currently, the ISA has approved 29 contractors with 15 year contracts locations all around the globe (ISA 2017). For example, India was granted an exclusive rights in 2017 for nodules found in a 75000 km<sup>2</sup> area that is thought to be able to yield 380 million tonnes of resources (nickel, copper, cobalt, and manganese) (ISA 2017). The environmental risks associated with these operations include large benthic disturbances, subsequent sediment plumes, and potential toxic waters in overlaying waters (Glover and Smith 2003; Halfar and Fujita 2007; Van Dover 2011).

Perhaps the largest impact in terms of resource extraction is the expansion of oil and gas into deeper water. Many oil companies began exploratory drilling sites in deepwater (125 to 1500 m deep) and ultra-deepwater (>1500 m deep) during the 1990s. These sites have propagated since then. According to the U.S. Environmental Protection Agency (EPA), the amount of deepwater and ultra-deepwater production has overtaken the shallow-water production of oil for the United States and other countries mining in deep waters (EPA 2016). The incentive to increase production into these deepwater areas, despite the increased risk and cost is due to higher prices for oil and government subsidies. The production in these deepwater and ultra deepwater regions is used to offset the decline in shallow-water reserves and maintaining the domestic oil industry in this country (U.S. MMS 2009). Both the number of platforms, as well as the number of barrels extracted has increased every year since 2006 (EPA 2016).

## **CLIMATE CHANGE**

Anthropogenic climate change is a major source of change in the environment, particularly with regards to the ramifications of increased oceanic temperatures (Barnett et al. 2005; Levitus et al. 2009; Hoegh-Guldberg and Bruno 2010). Reductions in primary production and shifts in phytoplankton populations are correlated with increases in sea surface temperatures (Gregg et al. 2003; Taucher and Oeschlies 2011). Changes from global climate change have the potential of disrupting deep-sea communities due to the

strong reliance of surface primary production for food supply (Ruhl and Smith 2004). Current domestic and international policies regarding climate change have focused on reducing carbon dioxide emissions from fossil fuel usage (Bierbaum et al. 2013; IPCC 2014). The international consensus is to attempt to keep the global temperature from rising an additional 2°C (IPCC 2014). Researchers have already found rising sea surface temperatures have expanded low chlorophyll waters, impacting the food supply for deep-sea communities (Polvino *et al.* 2008). These trends indicate additional increases in temperature may continue the expansion of low chlorophyll waters.

This study and other time-series research has provided evidence showing notable changes in deep-sea communities. It is less clear how often these shifts and population boom events occur. It is clear that holothurians can respond to changes in food supply faster than a yearly scale, a typical sampling scale. A single species can increase by two orders of magnitudes in a six-month period (Bett *et al.* 2001). This study shows how a large increase in population can last a few years depending on food supply and most likely, immigration and recruitment events. To gain a better understanding of climate change on population dynamics of the deep-sea communities, long-term time series are extremely important.

## REFERENCES

- Altman, N.S. 1992. An introduction to kernel and nearest-neighbor nonparametric regression. *The American Statistician* 46(3): 175-185
- Auster, P. J., and Langton, R. W. 1999. The effects of fishing on fish habitat. *American Fisheries Society Symposium*, 22: 150–187.
- Baker, K.D., J.A. Devine, and R.L. Haedrich. 2009. Deep-sea fishes in Canada's Atlantic: population declines and predicted recovery times. *Environmental Biology of Fishes* 85:79–88.
- Baldwin, R., R. Glatts, and K.L. Smith, JR. 1998. Particulate matter fluxes into the benthic boundary layer at a long timeseries station in the abyssal NE Pacific: Composition and fluxes. *Deep-Sea Res. II* 45: 643–665.
- Barnett, T.P., D.W. Pierce, K.M. AchutaRoa, P.J. Gleckler, B. D. Santer, J.M. Gregory, and W.M. Washington. 2005. Penetration of human-induced warming into the world's oceans. *Science* 309:284-287.
- Bett, B.J., M.G. Malzone, B.E. Narayanaswamy, and B.D. Wigham. 2001. Temporal variability in phytodetritus and megabenthic activity at the seabed in the deep Northeast Atlantic. *Progress in Oceanography* 50:349-368.
- Bierbaum, R.M. and P.A. Matson. 2013. Energy in the context of sustainability. *Daedalus*. 142(1): 146-161.
- Billett, D.S.M., B.J. Bett, A.L. Rice, M.H. Thurston, J. Galeron, M. Sibuet, and G A. Wolff. 2001. Long-term changes in the megabenthos of the Porcupine Abyssal Plain (NE Atlantic). *Progress in Oceanography* 50:325-348.
- Billett, D.S.M., B.J. Bett, W.D.K. Reid, B. Boorman, and I.G. Priede. Long-term change in the abyssal NE Atlantic: The '*Amperima* Event' revisited. *Deep Sea Research II* 57: 1406-1417.
- Bluhm, H., and A. Gebruk. 1999. Holothuroidea (Echinodermata) of the Peru Basin: ecological and taxonomic remarks based on underwater images. *Marine Ecology* 20:167-195.

- Bluhm, H., G. Schriever, and H. Thiel. 1995. Megabenthic recolonization in an experimentally disturbed abyssal manganese nodule area. *Marine Georesources Geotechnology* 13: 393-416.
- Boiman, O., E. Shechtman and M. Irani. 2008. In defense of Nearest-Neighbor based image classification. *IEEE Conference on Computer Vision and Pattern Recognition*, Anchorage, AK: 1-8.
- Boschen, R.E., P. C. Collins, V. Tunnicliffe, J. Carlsson, J.P.A. Gardner, J. Lowe, A. McCrone, A. Metaxas, F. Sinniger, A. Swaddling. 2016. A primer for use of genetic tools in selecting and testing the suitability of set-aside sites protected from deep-sea seafloor massive sulfide mining activities. *Ocean and Coastal Management* 122: 37-48.
- Bouland, C., C. Massin, and M. Janqoux. 1982. The fine structure of the buccal tentacles of *Holothuria forskali* (Echinodermata, Holothuroidea). *Zoomorphology* 101: 133-149.
- Bram, J. B., H.M. Page, and J.E. Dugan. 2005 Spatial and temporal variability in early successional patterns of an invertebrate assemblage at an offshore oil platform. *Journal of Experimental Marine Biology and Ecology* 317(2): 223-237.
- Cáceres, C.E. 1997. Dormancy in invertebrates. *Invertebrate Biology*. 116: 371-383.
- Costa, V., A. Mazzola, and S. Vizzini. 2014. *Holothuria tubulosa* Gmelin 1791 (Holothuroidea, Echinodermata) enhances organic matter recycling in *Posidonia oceanica* meadows. *Journal of Experimental Marine Biology and Ecology* 461: 226-232.
- Clark, P.J., and F.C. Evans. 1954. Distance to nearest neighbor as a measure of spatial relationships in populations. *Ecology* 35(4): 445-453.
- Clark, M. R., F. Althaus, T.A. Schlacher, A. Williams, D. A. Bowden, and A. A. Rowden. 2016. The impacts of deep-sea fisheries on benthic communities: a review. *ICES Journal of Marine Science* 73 (Supplement 1), i51 –i69.
- Ebert, T.A. 1978. Growth and Size of the tropical sea cucumber *Holothuria* (*Halodeima*) *atra* Jäger at Enewaetak Atoll, Marshall Islands. *Pacific Science* 32(2): 183-191.

- [EPA] Environmental Protection Agency. 2016. Offshore oil production in deepwater and ultra-deepwater is increasing. October 28, 2016. Accessed on March 27, 2018: <https://www.eia.gov/todayinenergy/detail.php?id=28552>
- [FAO] Food and Agriculture Organization of the United Nations. 2017. Management of Deep-Sea Fisheries in the High Seas. FAO, Rome, Italy.
- Gebruk, A.V. 1995. Locomotory organs in elapsipodid holothurians: functional-morphology and evolutionary approaches. *Echinoderm Research* 95-102.
- Glover, A.G., and C.R. Smith. 2003. The deep-sea floor ecosystem: current status and prospects of anthropogenic change by the year 2025. *Environmental Conservation* 30: 219-241.
- Grassle, J. F., H.L. Sanders, R.R. Hessler, G.T. Rowe, and T. McLellan. 1975. Pattern and zonation: a study of the bathyal megafauna using the research submersible Alvin. *Deep Sea Research I* 22: 457–481.
- Grassle, J.F. and L.S. Morse-Porteous. 1987. Macrofaunal colonization of disturbed deep-sea environments and the structure of deep-sea communities. *Deep-sea Research I* 34(12): 1911-1930.
- Gregg, W.W. M.E. Conkright, P. Ginoux, J.E. O'Reilly, and N.W. Casey. 2003. Ocean primary production and climate: Global decadal changes. *Geophysical Research Letters* 30(15) 1-4.
- Hansen, B. 1975. Systematic and biology of deep-sea holothurians. *Galathea Report* 13: 1-262.
- Halfar, J., R.M. Fujita. 2007. Danger of deep-sea mining. *Science* 316:987.
- Hoegh-Guldberg, O. and J.F. Bruno. 2010. The impact of climate change on the world's marine ecosystems. *Science* 328(5985): 1523-1528.
- Huffard, C.L., L.A. Kuhnz, L. Lemon, A.D. Sherman, and K.L. Smith Jr. 2016. Demographic indicators of change in a deposit-feeding abyssal holothurian community (Station M, 4000m), *Deep-sea Research I* 109: 27-39.
- Iken, K., T. Brey, U. Wand, I. Voigt, and P. Junghans. 2001. Food web structure of the benthic community at Porcupine Abyssal Plain (N. Atlantic): a stable isotope analysis. *Progress in Oceanography* 50: 383–405.

- [IPCC] Intergovernmental Panel on Climate Change. 2014. Climate change 2014: synthesis report. Contribution of working groups I, II and III to the fifth assessment report of the Intergovernmental Panel on Climate Change [Core Writing Team, R.K. Pachauri and L.A. Meyer (eds.)]. IPCC, Geneva, Switzerland, 1-151.
- [ISA] International Seabed Authority. 2017. Selected decisions and documents of the twenty-third session: 7-18 August 2017. Kingston, Jamaica. Accessed March 28, 2018:  
[https://www.isa.org.jm/sites/default/files/files/documents/en\\_3.pdf](https://www.isa.org.jm/sites/default/files/files/documents/en_3.pdf)
- Johnson, N.A., J.W. Campbell, T.S. Moore, M.A. Rex, R.J. Etter, C.R. McClain, and M.D. Dowell. 2007. The relationship between the standing stock of deep-sea macrobenthos and surface primary production in the western north Atlantic. *Deep-sea Research I* 54:1350-1360.
- Klanian, M.G. 2013. Physiological and immunological conditions of the sea cucumber *Isostichopus badionotus* (Selenka, 1867) during dormancy. *Journal of Experimental Marine Biology and Ecology* 444: 31-37.
- Kaufman, R.S. and K.L. Smith, Jr. 1997. Activity patterns of mobile epibenthic megafauna at an abyssal site in the eastern North Pacific: results from a 17-month time-lapse photographic study. *Deep-sea Research I* 44 (4): 559-579.
- Kelamer, B.P. and J.S. Levinton. 2003. Variation in detrital enrichment causes spatio-temporal variation in soft-sediment assemblages. *Marine Ecology Progress Series* 261: 85-97.
- Kiriakoulakis, K., E. Stutt, S.J. Rowland, A. Vangriesheim, R. S. Lampitt, and G.A. Wolff. 2001. Controls on the organic chemical composition of settling particles in the Northeast Atlantic Ocean. *Progress in Oceanography* 50: 65–87.
- Koslow, J.A., G.W. Boehlert, J.D.M. Gordon, R.L. Haedrich, P. Lorange, and N. Parin. 2000. Continental slope and deep-sea fisheries: implications for a fragile ecosystem. *ICES Journal of Marine Science* 57: 548-557.
- Kuhnz, L.A., H.A. Ruhl, C.L. Huffard and K.L. Smith Jr. 2014. Rapid changes and long-term cycles in the benthic megafaunal community observed over 24 years in the abyssal northeast Pacific. *Progress in Oceanography* 124: 1-11.

- Lampitt, R. S., B.J. Bett, K. Kiriakoulakis, E.E. Popova, O. Ragueneau, A. Vangrieshem, and G.A. Wolff. 2001. Material supply to the abyssal seafloor in the Northeast Atlantic. *Progress in Oceanography* 50: 27–63.
- Lauerman, L.M.L., R.S. Kaufmann, and K.L. Smith, Jr. 1996. Distribution and abundance of epibenthic megafauna at a long time-series station in the abyssal northeast Pacific. *Deep-sea Research I* 43:1075-1104.
- Lauerman, L.M.L., J.M. Smoak, T. J. Shaw, W.S. Moore, and K.L. Smith. 1997.  $^{234}\text{Th}$  and  $^{210}\text{Pb}$  evidence for rapid ingestion of settling particles by mobile epibenthic megafauna in the abyssal NE Pacific. *Limnology and Oceanography* 42(3): 589-595.
- Levitus, S. J.I. Antonov, T.P. Boyer, R.A. Locarnini, H.E. Garcia, and A.V. Mishonov. 2009. Global ocean heat content 1955-2008 in light of recently revealed instrumentation problems. *Geophysical Research Letters* 36: L07608.
- Lodge, M., D. Johnson, G. LeGurun, M. Wengler, P. Weaver, and V. Gunn. 2014. Seabed mining: International Seabed Authority environmental management plan for the Clarion-Clipperton Zone. A partnership approach. *Marine Policy* 49L 66-72.
- Massin, C. 1982. Food and feeding mechanisms: Holothuroidea. In: Jangoux M and Lawrence JM (eds), *Echinoderm Nutrition*, Balkema Publ Rotterdam, 43-55.
- Michio K., K. Kengo, K. Yasunori, M. Hitoshi, Y. Takayuki, Y. Hideaki and S. Hiroshi. 2003. Effects of deposit feeder *Stichopus japonicus* on algal bloom and organic matter contents of bottom sediments of the enclosed sea. *Marine Pollution Bulletin* 47: 118–125.
- Miller, J.E., and D.L. Pawson. 1990. Swimming sea cucumbers (Echinodermata: Holothuroidea): a survey with analysis of swimming behavior in four bathyal species. *Smithsonian Contributions to the Marine Sciences* 35: 1–18.
- Miller, R.J., C.R. Smith, D.J. Demaster, and W.L. Fornes. 2000. Feeding selectivity and rapid particle processing by deep-sea megafaunal deposit feeders: A  $^{234}\text{Th}$  tracer approach. *Journal of Marine Research* 58: 653-673.
- Morato, T., T.J. Pitcher, M.R. Clark, G. Menezes, F. Tempera, F. Porteiro, E. Giacomello, E., and R.S. Santos. 2010. Can we protect seamounts for research? A call for conservation. *Oceanography* 23: 190–199.

- Morrisey D.J., L. Howitt, A. J. Underwood, and J.S. Stark. 1992. Spatial variation in soft-sediment benthos. *Marine Ecological Progress Series* 81:197–204.
- Moore, H.M. 1994. Feeding and bioaccumulation of trace metals in deep-sea holothurians. Queen's University, Belfast.
- Norcross, B.L. and F. J. Meuter. 1999. The use of an ROV in the study of juvenile fish. *Fisheries Research* 39: 241-251.
- Page, H.M., J. E. Dugan, D. S. Dugan, J. B. Richards, D.H. Hubbard. 1999. Effects of an offshore oil platform on the distribution and abundance of commercially important crab species. *Marine Ecology Progress Series* 185: 47-57.
- Pauly, D., J. Alder, E. Bennett, V. Christensen, P. Tyedmers P, and R. Watson. 2003 The future for fisheries. *Science* 302(5649):1359–61.
- Pawson, D.L. and E.J. Foel. 1986. *Peniagone leander* new species, an abyssal benthopelagic sea cucumber (Echinodermata: Holothuroidea) from the eastern Central Pacific Ocean. *Bulletin of Marine Science* 38: 293–299.
- Pitcher, T.J., M.R. Clark, T. Morato, and R. Watson. 2010. Seamount fisheries: do they have a future? *Oceanography* 23: 134–144.
- Polvino, J.J., E.A. Howell, and M. Abecassis. 2008. Ocean's least productive waters are expanding. *Geophysical Research Letters* 35:L03618.
- Pyper, B.J., and R. M. Peterman. 1998. Comparison of methods to account for autocorrelation in correlation analyses of fish data. *Canadian Journal of Fisheries and Aquatic Sciences* 55: 2127-2140.
- R Core Team (2013). R: A language and environment for statistical computing. R Foundation for Statistical Computing, Vienna, Austria. URL: <http://www.R-project.org/>
- Rex, M.A. 1981. Community structure in deep-sea benthos. *Annual Review of Ecology and Systematics* 12: 331-353.
- Rhoads, D.C., P.L. McCall, and J.Y. Yingst. 1978. Disturbance and production on estuarine seafloor. *American Scientist* 66: 577–586.
- Roberts, D. 1979. Deposit-feeding mechanisms and resource partitioning in tropical holothurians. *Journal of Experimental Marine Biology and Ecology* 37(1): 43-56.

- Roberts, D., A. Gebruk, V. Levin, and B.A.D. Manship. 2000. Feeding and digestive strategies in deposit-feeding holothurians. *Oceanography and Marine Biology: An Annual Review* 38: 257-310.
- Rogacheva, A., A. Gebruk, and C. H. S. Alt. 2012. Swimming deep-sea holothurians (Echinodermata: Holothuroidea) on the northern Mid-Atlantic Ridge. *Zoosymposia* 7: 213-229.
- Ruhl, H.A. 2007. Abundance and size distribution dynamics of abyssal epibenthic megafauna in the northeast Pacific. *Ecology* 88(5): 1250-1262.
- Ruhl, H.A. and K.L. Smith. 2004. Shifts in deep-sea community structure linked to climate and food supply. *Science* 305: 513-515.
- Schlining, B.M. and N. J. Stout. 2006. MBARI's Video Annotation and Reference System. Oceans Boston, MA.
- Scott, S.D. 2001. Deep ocean mining. *Geoscience Canada* 28(2): 87-96.
- Sherman, A.D. and K.L. Smith. 2009. Deep-sea benthic boundary layer communities and food supply: a long term monitoring strategy. *Deep-sea Research II* 56: 1754-1762.
- Smith Jr., K.L., Jr. 1992. Benthic boundary layer communities and carbon cycling at abyssal depths in the central North Pacific. *Limnology and Oceanography* 37:1034-1056.
- Smith Jr., K.L., R.S. Kaufmann, and W.W. Wakefield. 1993. Mobile megafaunal activity monitored with a time-lapse camera in the abyssal North Pacific. *Deep-Sea Research I*: 40(11/12): 2307-2324.
- Smith Jr., K.L. and E.R.M. Druffel. Long time-series monitoring of an abyssal site in the NE Pacific: an introduction. *Deep-Sea Research II* 45: 573-586.
- Smith Jr., K.L. and R.S. Kaufmann. 1999. Long-term discrepancy between food supply and demand in the deep eastern North Pacific. *Science* 285(5417): 1174-1177.
- Smith Jr., K.L., R.J. Baldwin, H.A. Ruhl, M. Kahru, B.G. Mitchell, and R.S. Kauffman. 2006. Climate effect on food supply to depths greater than 4,000 meters in the north Pacific. *Limnology and Oceanography* 51(1): 166-176.

- Smith Jr., K.L., H.A. Ruhl, B.J. Bett, D.S.M. Billett, R.S. Lampitt, and R.S. Kauffman. 2009. Climate, carbon cycling, and deep-ocean ecosystems. *Proceedings of the National Academy of Sciences* 106(46): 19211-19218.
- Smith Jr., K.L., A.D. Sherman, P. R. McGill, R.G. Henthorn, J. Ferreira, and C.L. Huffard. 2017. Evolution of monitoring an abyssal time-series station in the N.E. Pacific over 28 years. *Oceanography* 30(4): 72-81.
- Stoner, A., C.H. Ryer, S.J. Parker, P.J. Auster, and W.W. Wakefield. 2008. Evaluating the role of fish behavior in surveys conducted with underwater vehicles. *Canadian Journal of Fisheries and Aquatic Sciences* 65(6): 1230-1243.
- Strickland, J.D. and T.R. Parsons. 1972. A practical handbook of seawater analysis.
- Sweetman, A.K., and U. Witte. 2008. Response of an abyssal macrofaunal community to a phytodetrital pulse. *Marine Ecological Progress Series* 355: 73-84.
- Taucher, J. and A. Oschlies. 2011. Can we predict the direction of marine primary production change under global warming? *Geophysical Research Letters* 38(2): L02603.
- Thiel, H., H. Bluhm, C. Borowski, C. Bussau, A.J. Gooday, C. Maybury, and G. Schriever. 1992. The impact of mining on deep sea organisms. The DISCOL-Project. *Ocean Challenge* 3(1): 40-46.
- Thrush, S.F. 1991. Spatial patterns in soft-bottom communities. *Trends in Ecology and Evolution* 6:75-79.
- Thrush, S.F., R. B. Whitlatch, R.D. Pridmore, J.E. Hewitt, V.J. Cummings, and M.R. Wilkinson. 1996. Scale-dependent recolonization: the role of sediment stability in a dynamic sandflat habitat. *Ecology* 77: 2472-2487.
- [U.S. MMS] United States Minerals Mangement Service. 2009. Gulf of Mexico oil and gas production forecast 2009-2018; OCS Report MMS 2009-012. New Orleans, Louisiana, May 2009.
- Uthicke, S., B. Schaffelke, and M. Byrne. 2009. A boom-bust phylum? Ecological and evolutionary consequences of density variations in echinoderms. *Ecological Mongraphs* 79(1): 3-24.
- Van Dover, C.L. 2011. Tighten regulations on deep-sea mining. *Nature* 470: 31-33.

- Vardaro, M.F., D. Parmley, and K.L. Smith, Jr. 2007. A study of possible “reef effects” caused by a long-term time-lapse camera in the deep North Pacific. *Deep-Sea Research I* 54: 1231-1240.
- Wigham, B.D., P.A. Tyler, and D.S.M. Billett. 2003. Reproductive biology of the abyssal holothurian *Amperima rosea*: an opportunistic response to variable flux of surface derived organic matter? *Journal of the Marine Biological Association of the United Kingdom* 83:175–188.

**APPENDIX A**  
**SUPPLEMENTAL POPULATION DENSITY GRAPHS**  
**BY SPECIES**

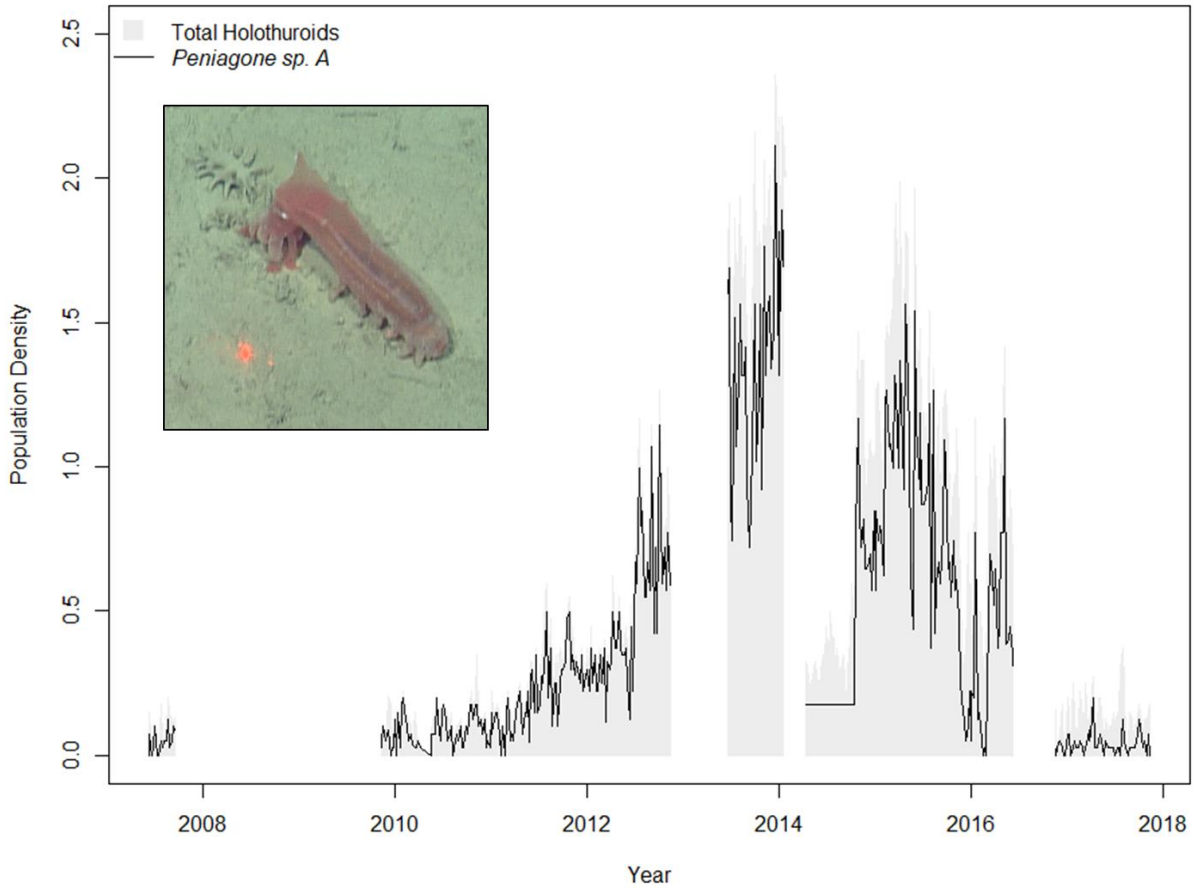


**Figure A-1.** Weekly population density of *Peniagone sp. A* (individuals/ m<sup>2</sup>) for time period between 2007 to 2017 in comparison to the total abundance of all species. NOTE: Image shows *Elpidia sp. A* (left) in addition to *Peniagone sp. A*.

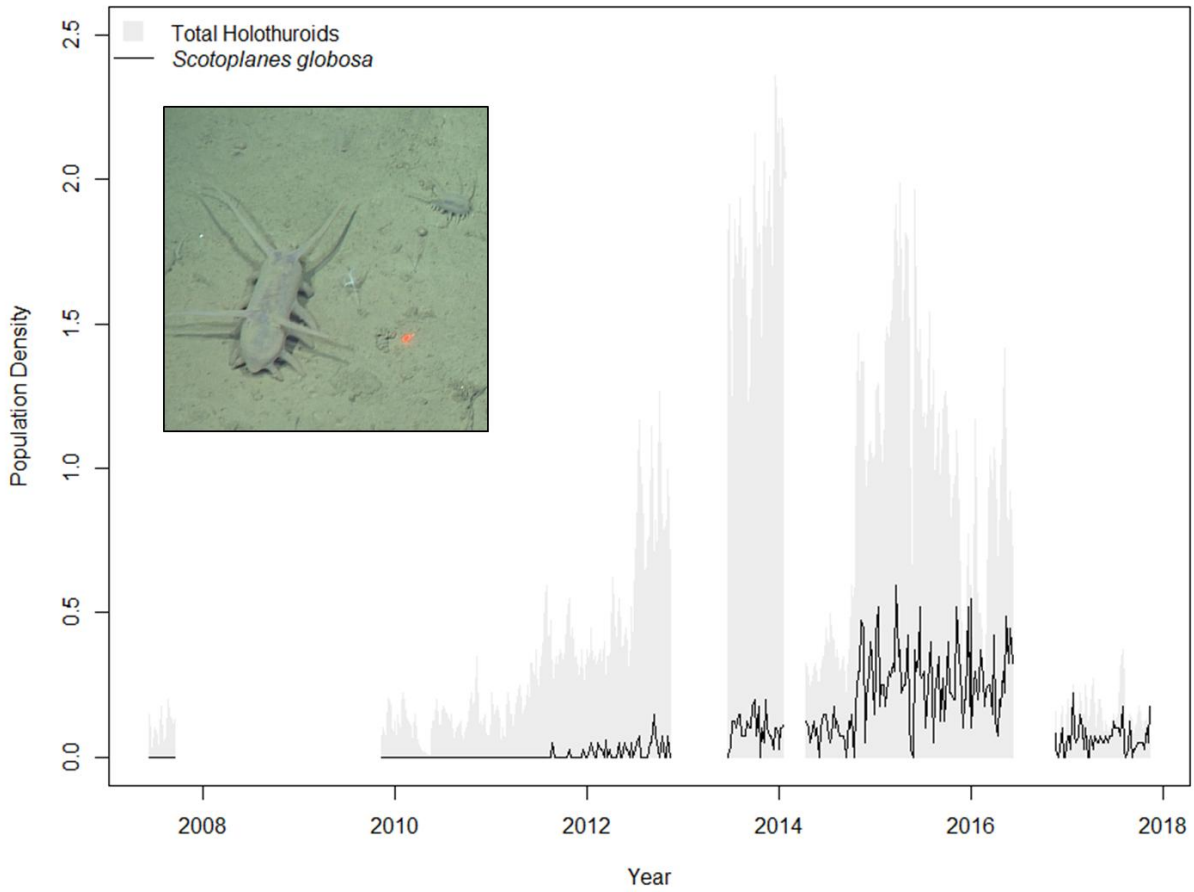


**Figure A-2.** Weekly population density of *Scotoplanes globosa* (individuals/ m<sup>2</sup>) for time period between 2007 to 2017 in comparison to the total abundance of all species.

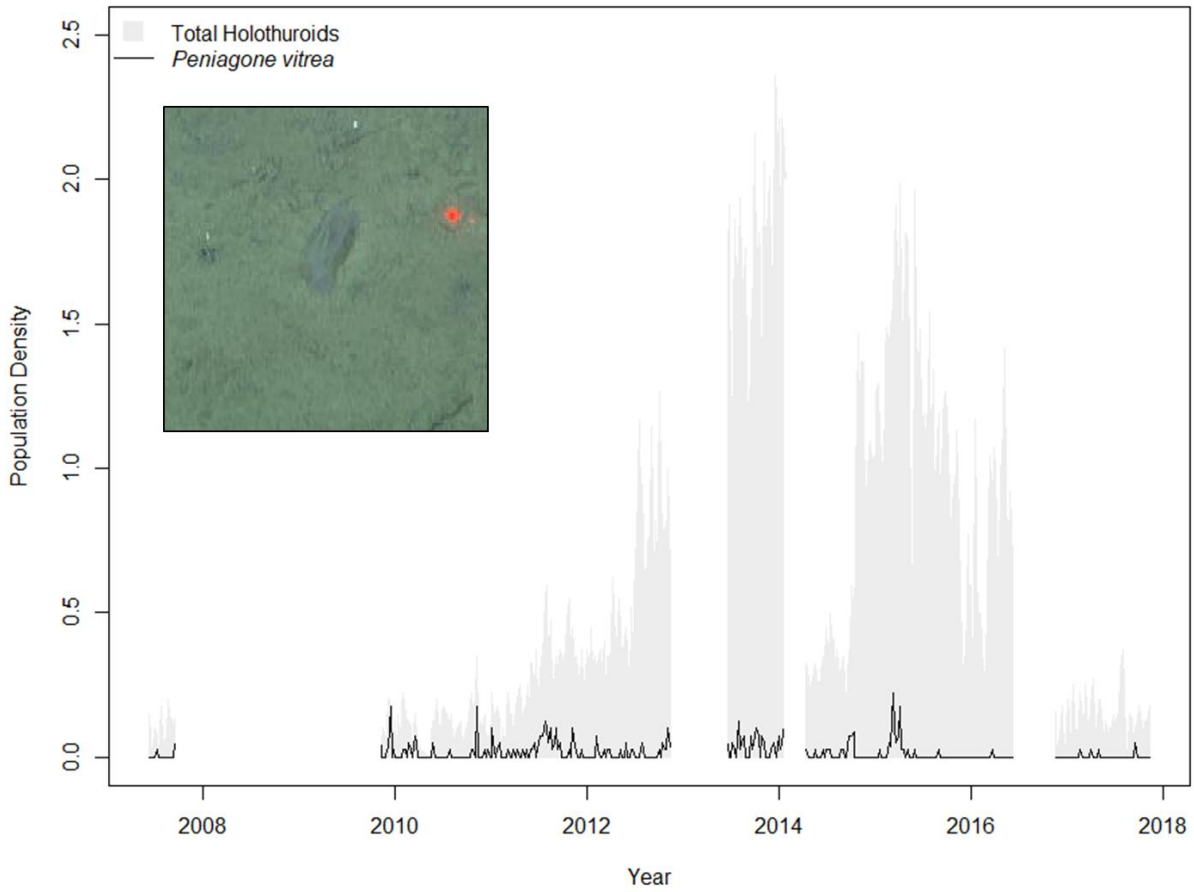


**Figure A-3.** Weekly population density of *Peniagone vitrea* (individuals/ m<sup>2</sup>) for time period between 2007 to 2017 in comparison to the total abundance of all species.

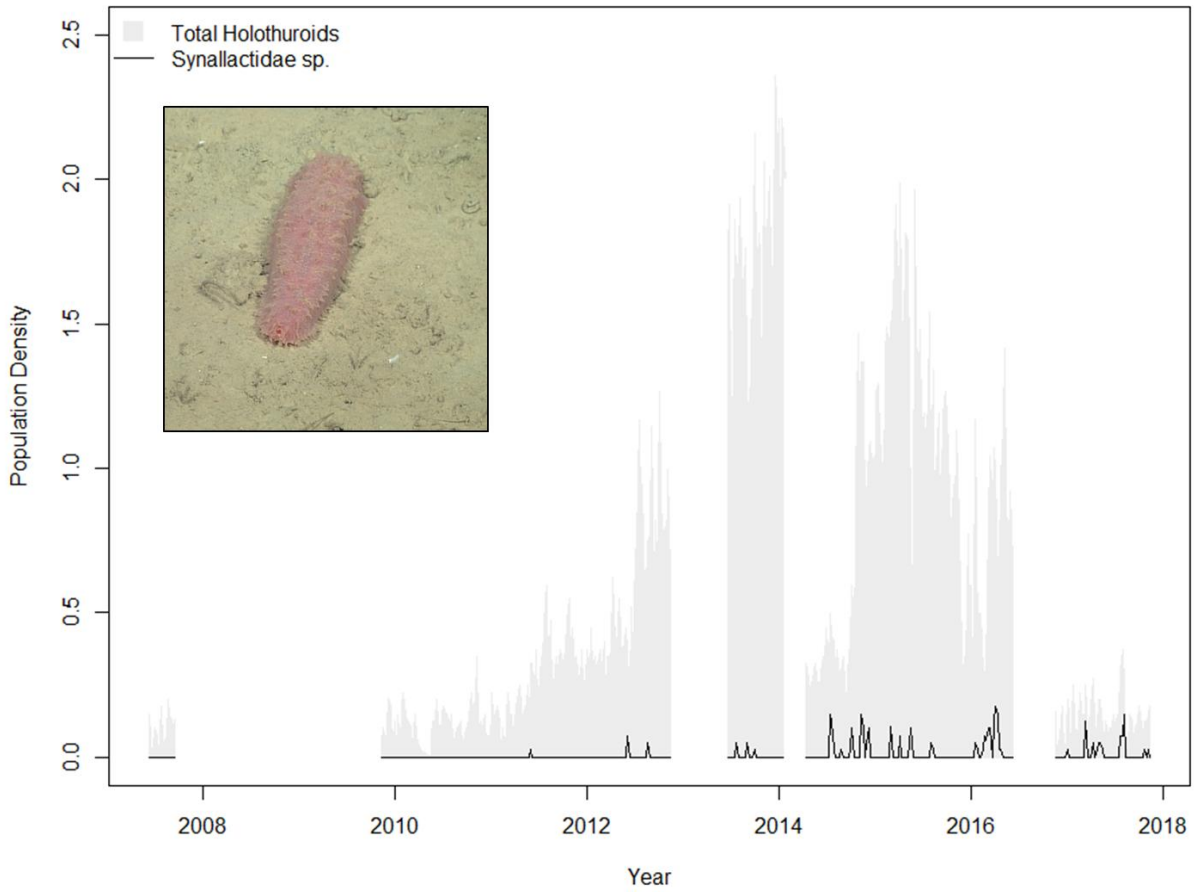


**Figure A-4.** Weekly population density of *Synallactidae* sp. (individuals/ m<sup>2</sup>) for time period between 2007 to 2017 in comparison to the total abundance of all species.

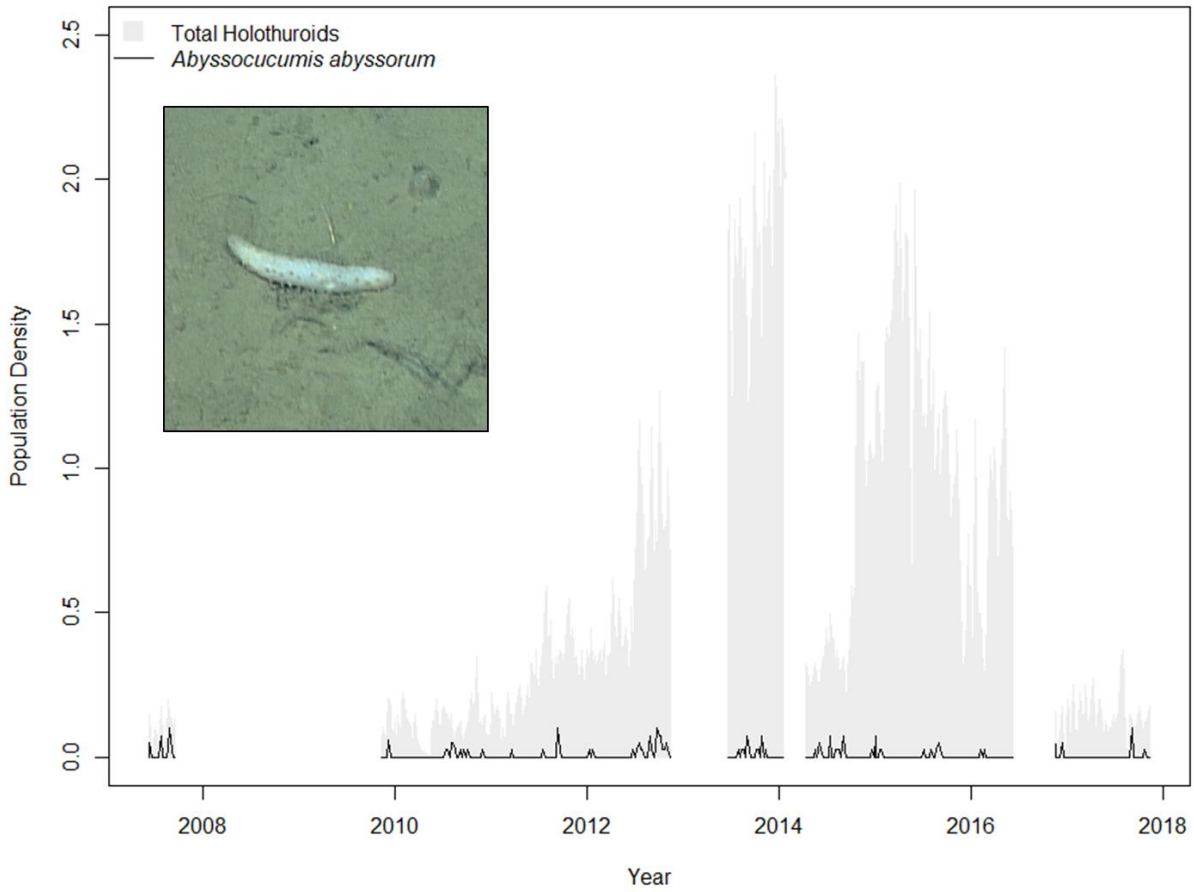


**Figure A-5.** Weekly population density of *Abyssocucumis abyssorum* (individuals/ m<sup>2</sup>) for time period between 2007 to 2017 in comparison to the total abundance of all species.

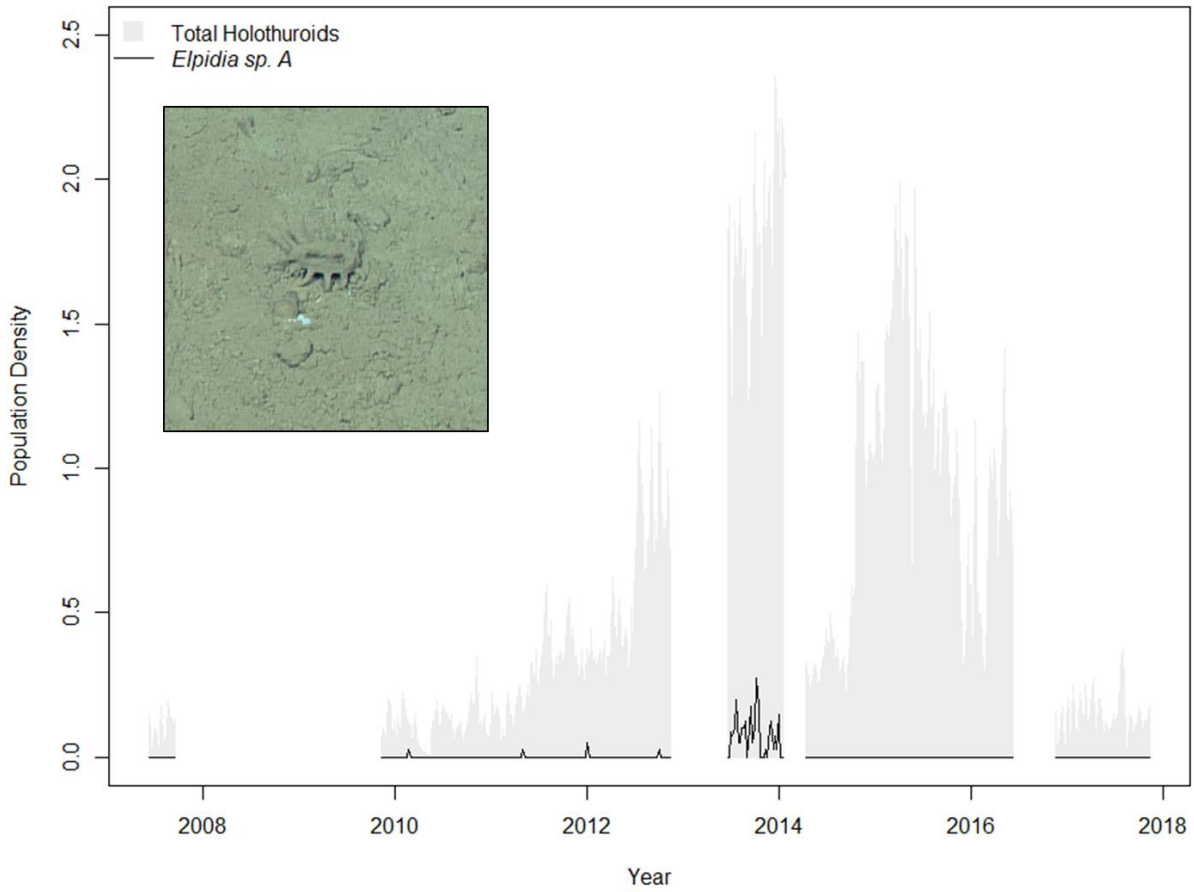


**Figure A-6.** Weekly population density of *Elpidia sp. A* (individuals/ m<sup>2</sup>) for time period between 2007 to 2017 in comparison to the total abundance of all species.

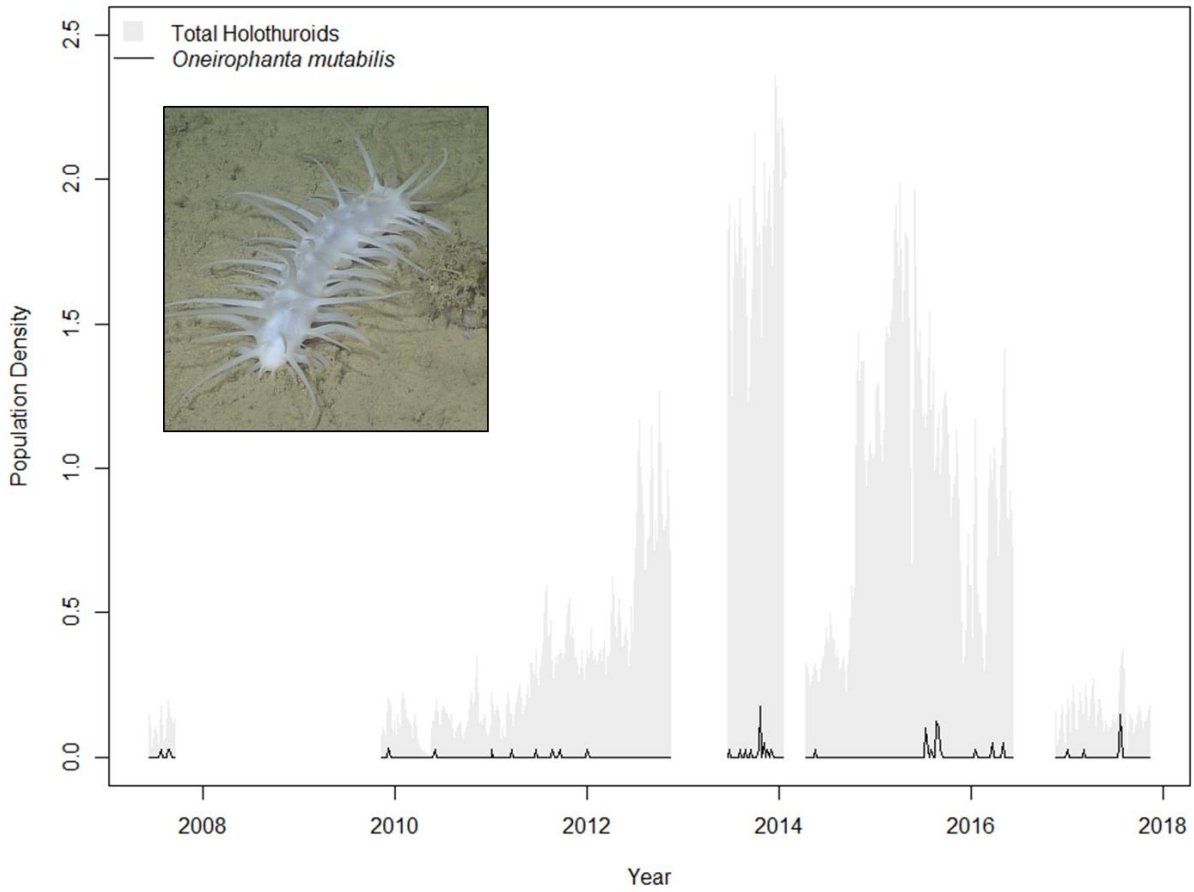


**Figure A-7.** Weekly population density of *Oneirophanta mutabilis* (individuals/ m<sup>2</sup>) for time period between 2007 to 2017 in comparison to the total abundance of all species.

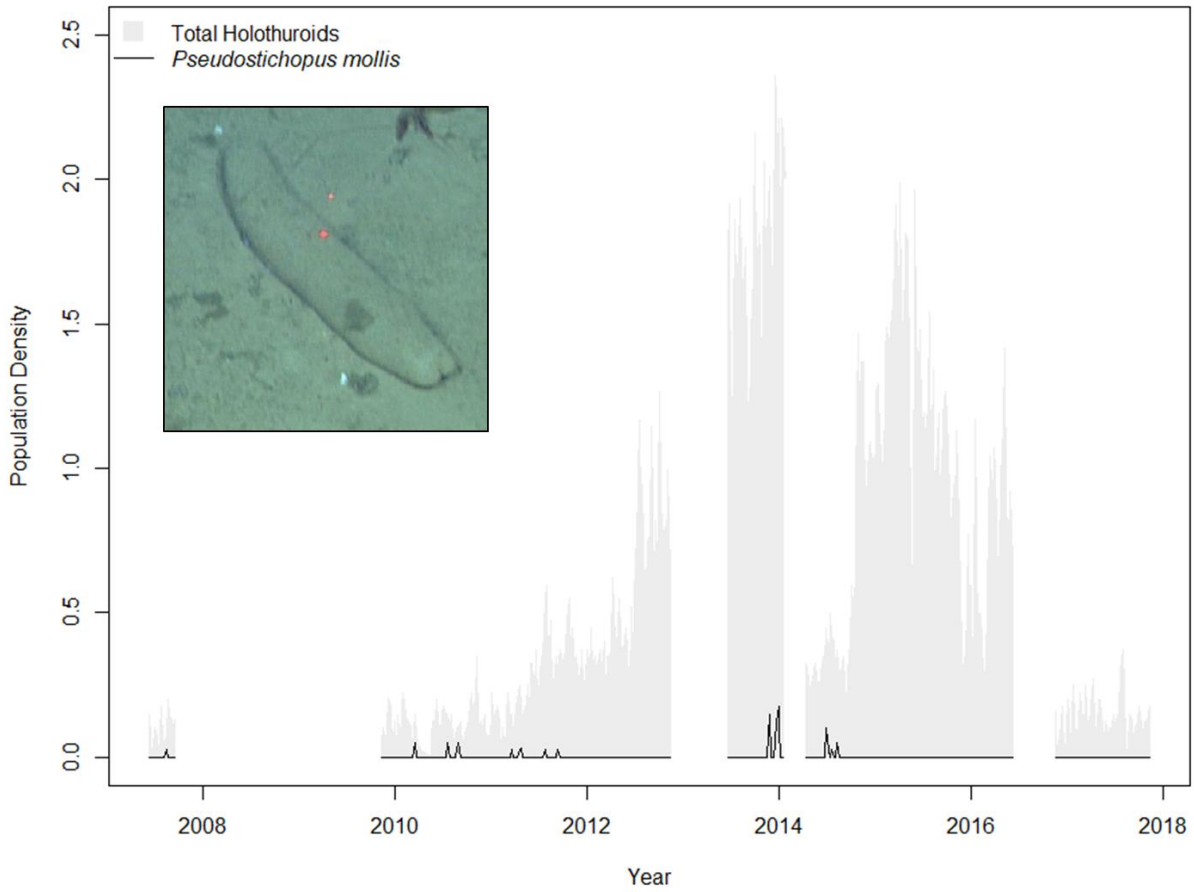


**Figure A-8.** Weekly population density of *Pseudostichopus mollis* (individuals/ m<sup>2</sup>) for time period between 2007 to 2017 in comparison to the total abundance of all species.

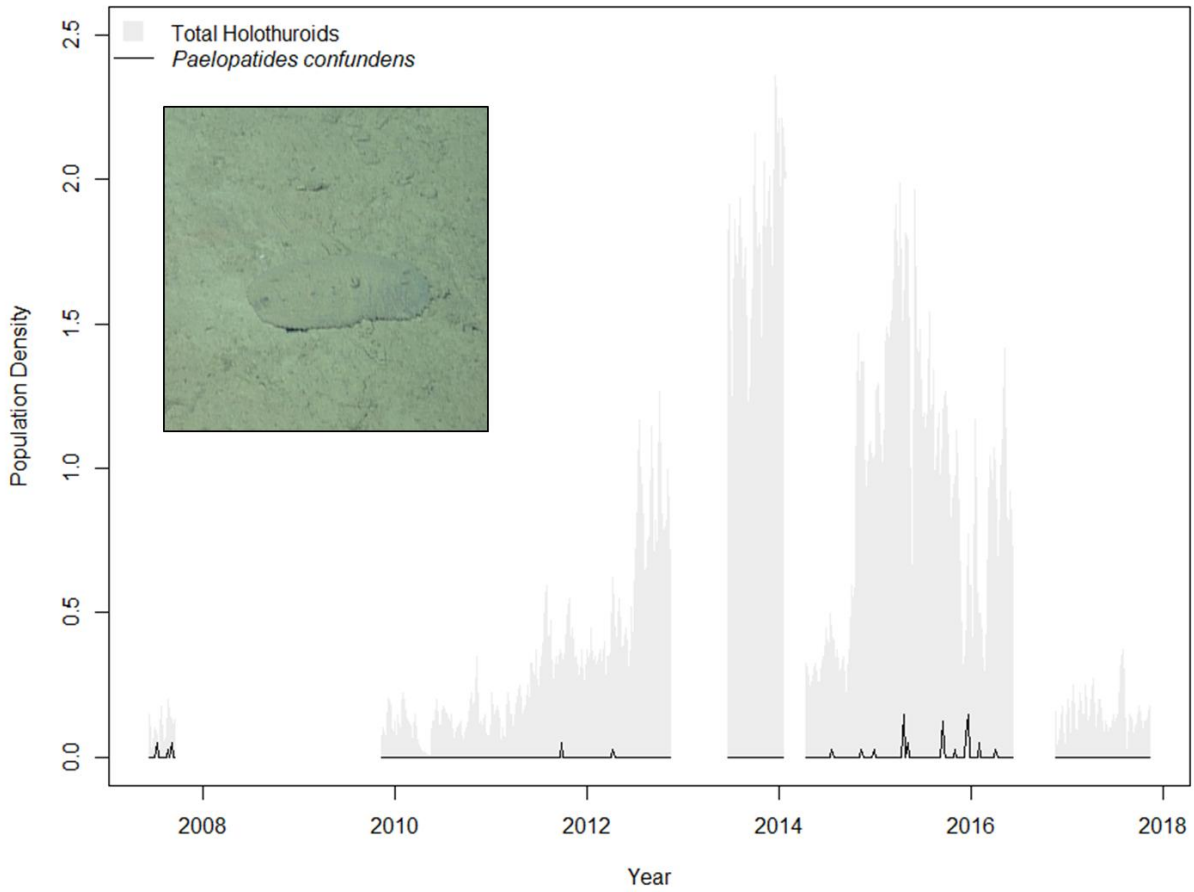


**Figure A-9.** Weekly population density of *Paelopatides confundens* (individuals/ m<sup>2</sup>) for time period between 2007 to 2017 in comparison to the total abundance of all species.

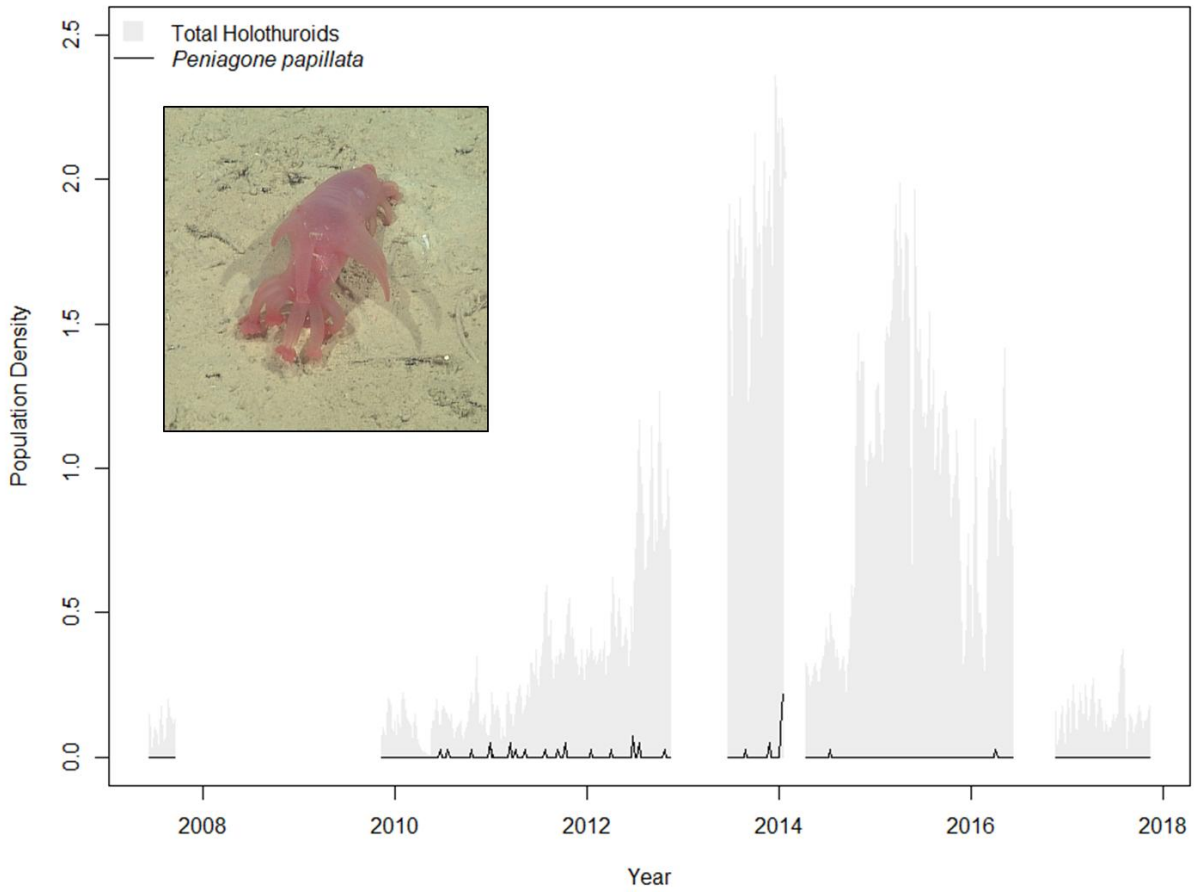


**Figure A-10.** Weekly population density of *Peniagone papillata* (individuals/ m<sup>2</sup>) for time period between 2007 to 2017 in comparison to the total abundance of all species.

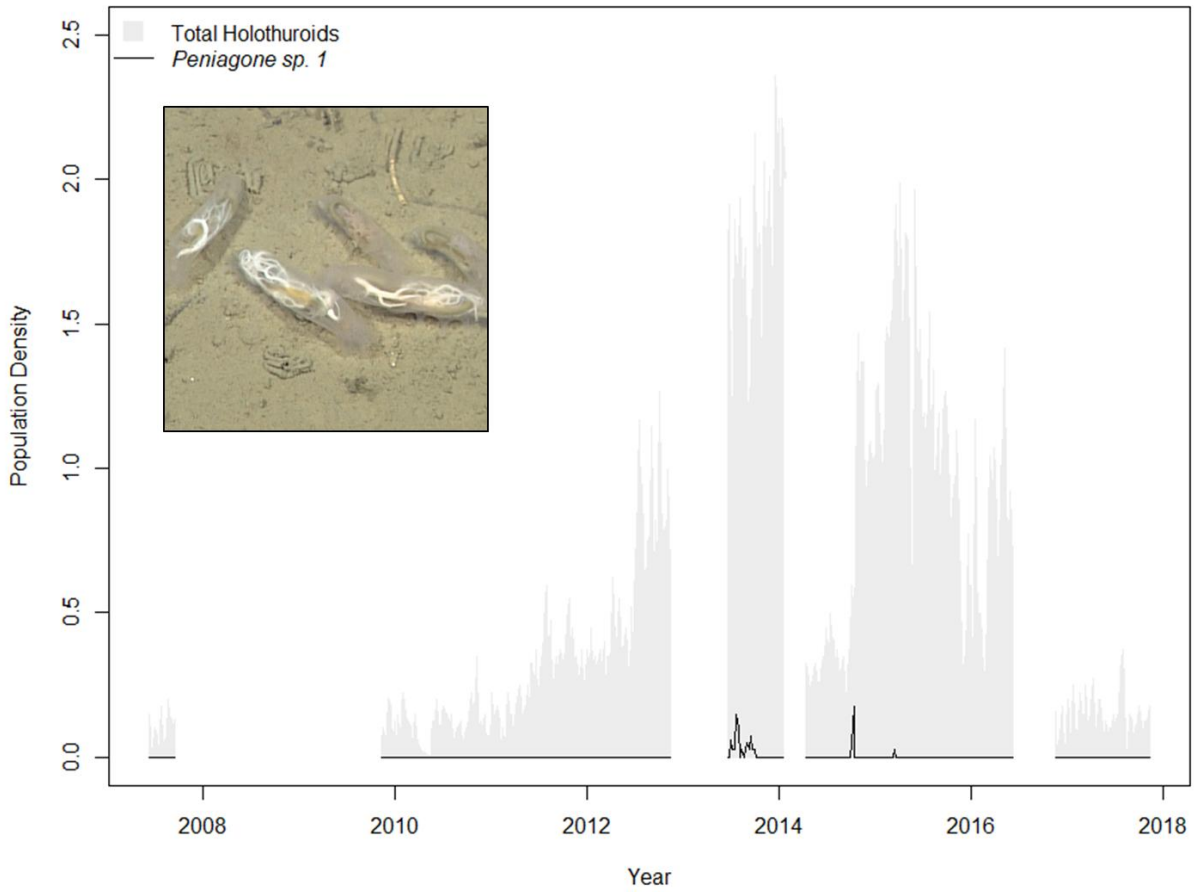


**Figure A-11.** Weekly population density of *Peniagone sp. 1* (individuals/ meter<sup>2</sup>) for time period between 2007 to 2017 in comparison to the total abundance of all species.

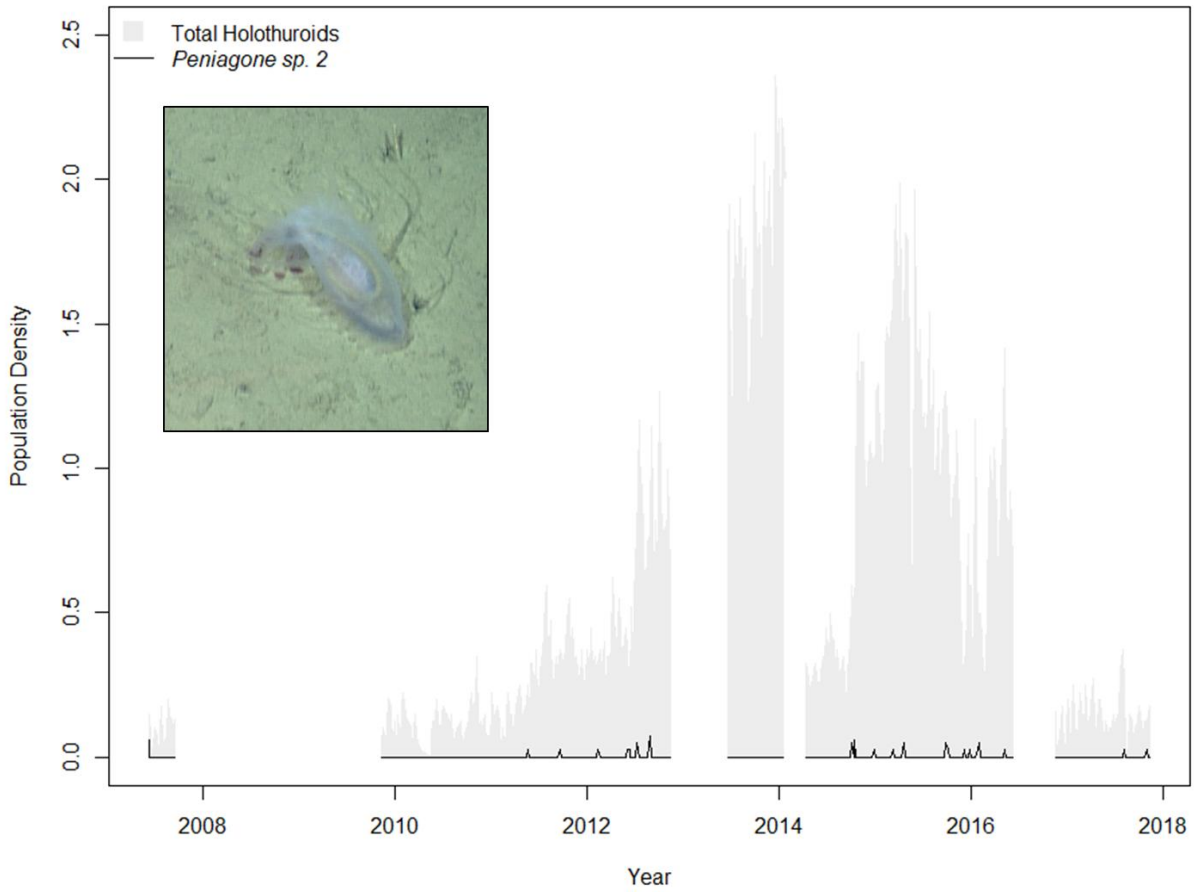


**Figure A-12.** Weekly population density of *Peniagone sp. 2* (individuals/ meter<sup>2</sup>) for time period between 2007 to 2017 in comparison to the total abundance of all species.

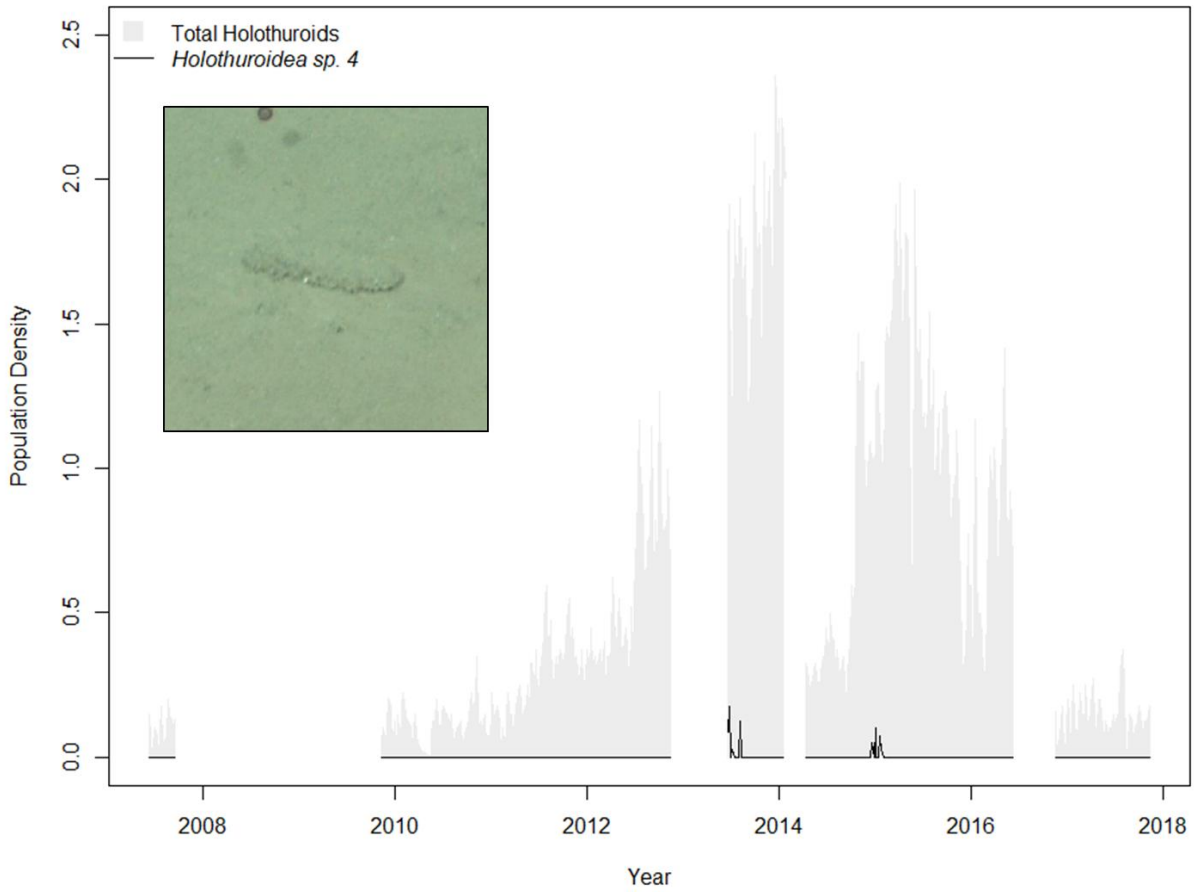


**Figure A-13.** Weekly population density of *Holothuroidea* sp. 4 (individuals/ m<sup>2</sup>) for time period between 2007 to 2017 in comparison to the total abundance of all species.

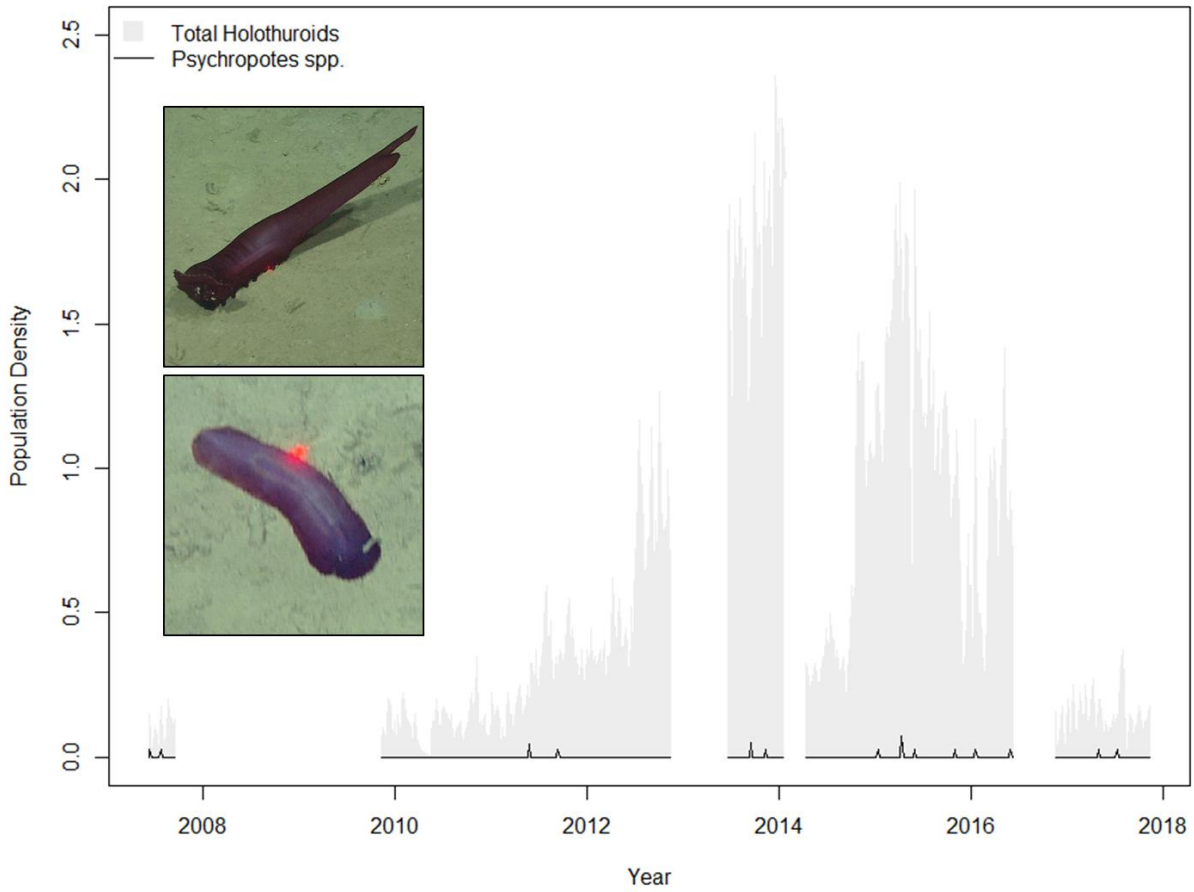


**Figure A-14.** Weekly population density of *Psychropotes* spp. (combination of *P. depressa* and *P. longicauda*) (individuals/ m<sup>2</sup>) for time period between 2007 to 2017 in comparison to the total abundance of all species.

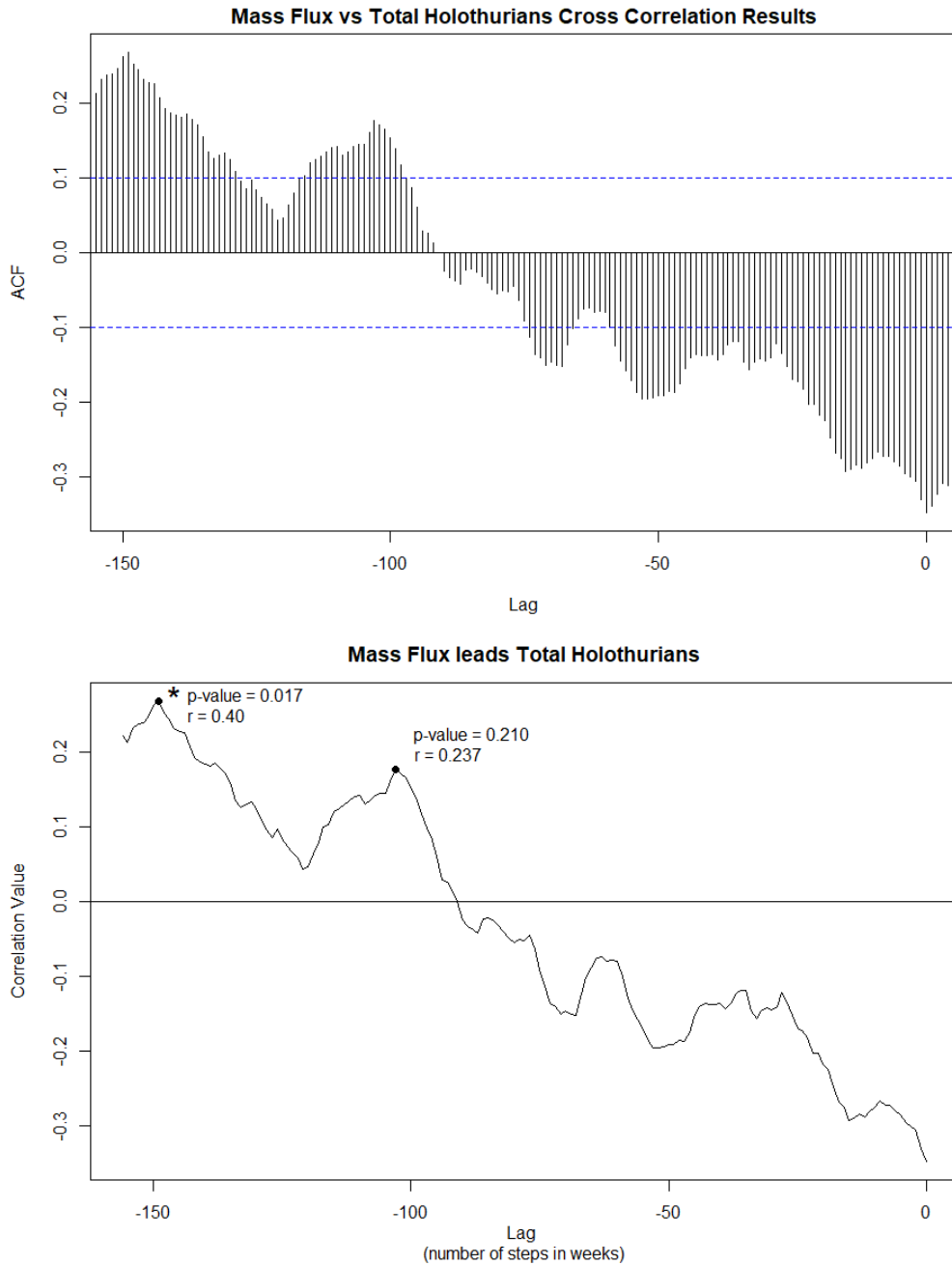
**Table A- 1.** Mean population density for each species by deployment. Bold numbers denote maximum density observed.

Deployment	<i>Peniagone</i>	<i>Scotoplanes</i>	<i>Peniagone</i>	Synallactidae	<i>Abyssocucumis</i>	unknown	<i>Elpidia</i> sp.	<i>Oneirophanta</i>
	sp. A	<i>globosa</i>	<i>vitrea</i>	gen.*	<i>abyssorum</i>	<i>Peniagone</i> sp.	A	<i>mutabilis</i>
52	0.048	0.000	0.004	0.000	0.017	0.002	0.000	0.005
55	0.066	0.000	0.024	0.000	0.002	0.001	0.001	0.001
56	0.093	0.000	0.005	0.000	0.010	0.000	0.000	0.001
57	0.110	0.000	0.019	0.000	0.002	0.000	0.001	0.002
58	0.275	0.003	<b>0.043</b>	0.001	0.006	0.002	0.000	0.003
59	0.308	0.015	0.010	0.002	0.002	0.006	0.002	0.001
60	0.651	0.032	0.017	0.002	<b>0.028</b>	0.004	0.001	0.000
62	1.378	<b>0.094</b>	0.039	0.004	0.010	<b>0.061</b>	<b>0.072</b>	<b>0.012</b>
63	<b>0.174</b>	0.091	0.019	0.016	0.012	0.001	0.000	0.001
64	0.927	0.284	0.022	0.019	0.004	0.002	0.000	0.000
65	0.799	0.238	0.001	0.004	0.007	0.000	0.000	0.020
66	0.362	0.277	0.001	<b>0.028</b>	0.002	0.001	0.000	0.004
67	0.031	0.065	0.001	0.007	0.007	0.000	0.000	0.002
68	0.044	0.063	0.003	0.016	0.004	0.000	0.000	0.005

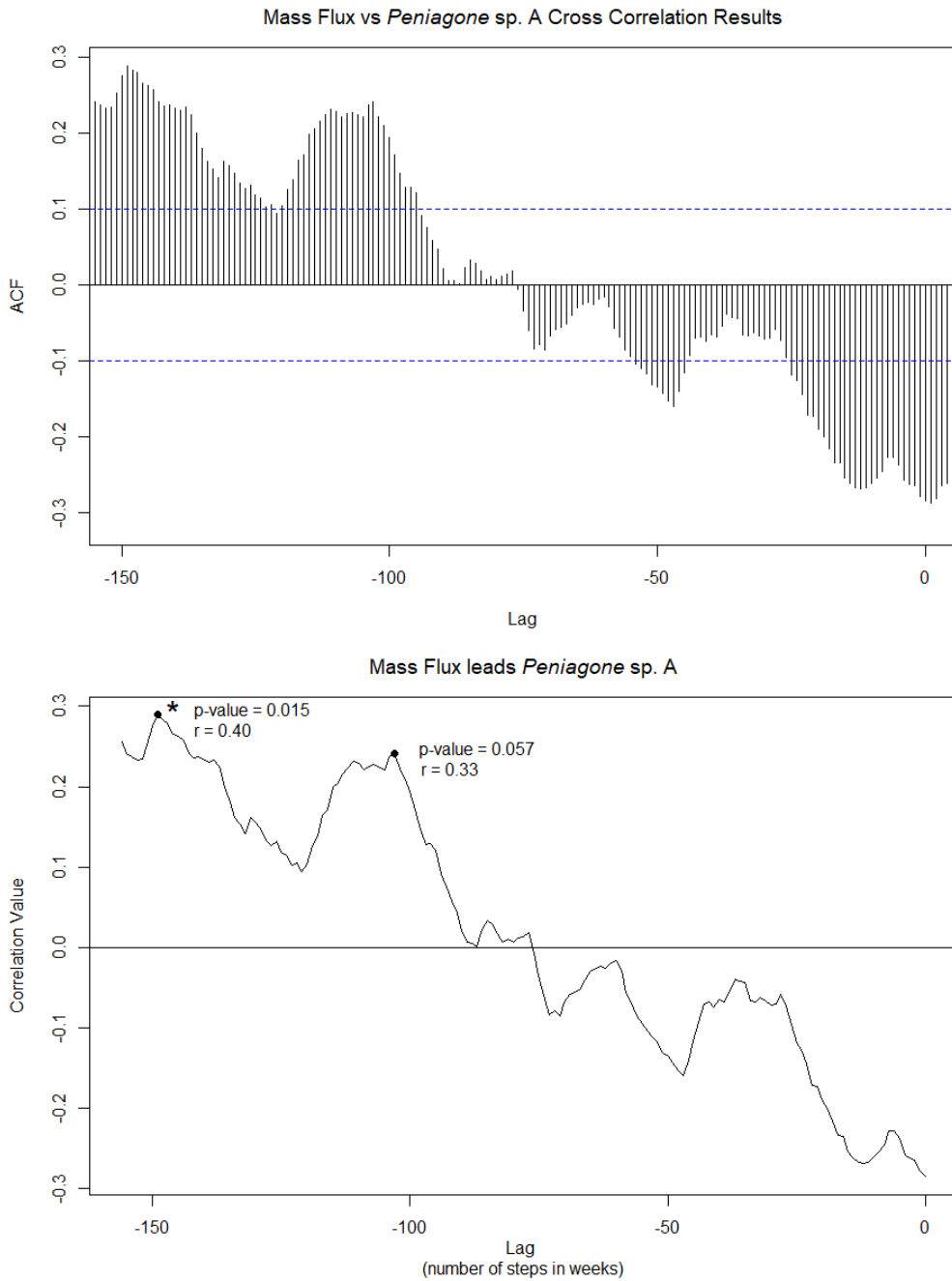
  

	<i>Pseudostichopus</i>	<i>Paelopatides</i>	<i>Peniagone</i>	<i>Peniagone</i> sp.	<i>Peniagone</i>	Holothuroidea	<i>Psychropotes</i>
	<i>mollis</i>	<i>confundens</i>	<i>papillata</i>	1	sp. 2	sp. 4	spp.
52	0.002	0.008	0.000	0.000	0.004	0.000	0.0031
55	0.002	0.000	0.000	0.000	0.000	0.000	0.000
56	0.005	0.000	0.003	0.000	0.000	0.000	0.000
57	0.003	0.000	0.006	0.000	0.001	0.000	0.000
58	0.002	0.002	0.004	0.000	0.001	0.000	0.0026
59	0.000	0.001	0.002	0.000	0.002	0.000	0.000
60	0.000	0.000	0.006	0.000	<b>0.0054</b>	0.000	0.000
62	<b>0.018</b>	0.000	<b>0.017</b>	<b>0.018</b>	0.000	<b>0.012</b>	0.002
63	0.007	0.001	0.001	0.008	0.002	0.000	0.000
64	0.000	0.007	0.000	0.001	0.004	0.007	<b>0.0033</b>
65	0.000	0.0087	0.000	0.000	0.004	0.000	0.001
66	0.000	<b>0.0090</b>	0.001	0.000	0.0045	0.000	0.002
67	0.000	0.007	0.000	0.000	0.000	0.000	0.000
68	0.000	0.000	0.000	0.000	0.001	0.000	0.001

**APPENDIX B**  
**SUPPLEMENTAL CROSS CORRELATION GRAPHS**  
**(SPECIES VS. MASS FLUX)**



**Figure B-1.** Cross correlation results for total holothurians. Lag in time series data. Positive correlation peaks (first and maximum) examined. Corrections for autocorrelation reflected in correlation values ( $r$ ) and p-values.



**Figure B-2.** Cross correlation results for *Peniagone* sp. A. Lag in time series data. Positive correlation peaks (first and maximum) examined. Corrections for autocorrelation reflected in correlation values ( $r$ ) and p-values.

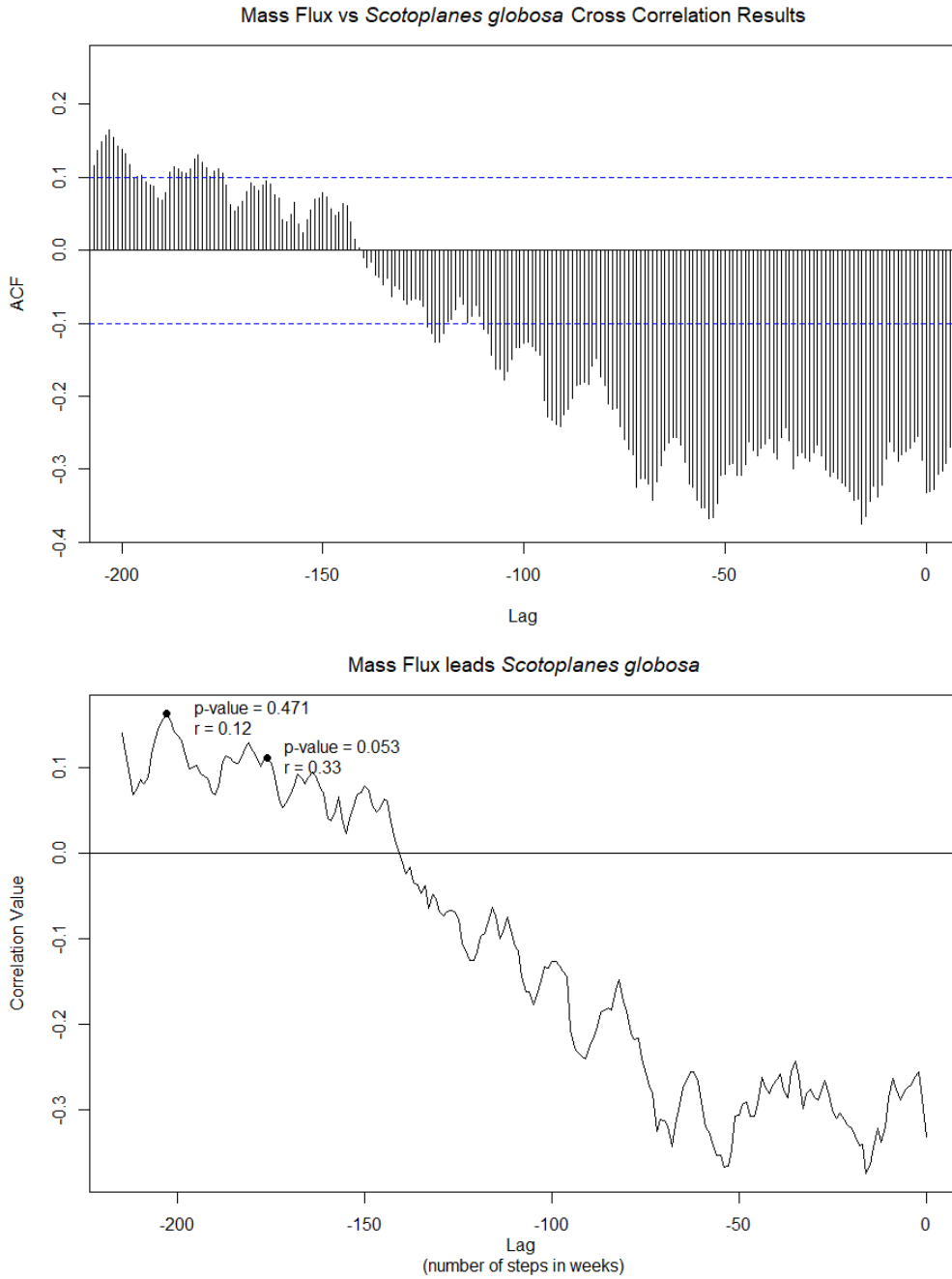


**Figure B-3.** Cross correlation results for *Scotoplanes globosa*. Lag in time series data. Positive correlation peaks (first and maximum) examined. Corrections for autocorrelation reflected in correlation values (r) and p-values.

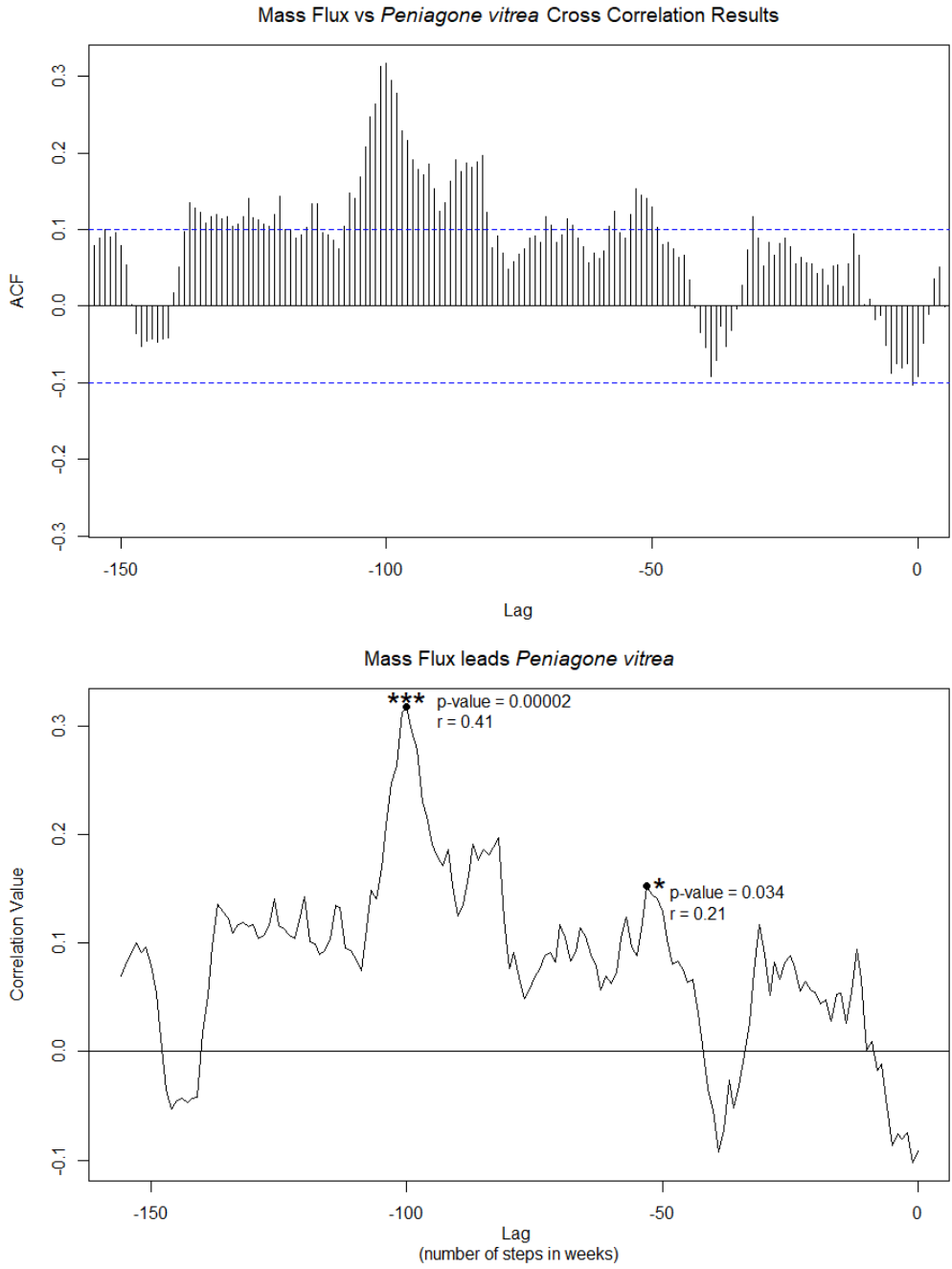


**Figure B-4.** Cross correlation results for *Peniagone vitrea*. Lag in time series data. Positive correlation peaks (first and maximum) examined. Corrections for autocorrelation reflected in correlation values (r) and p-values.

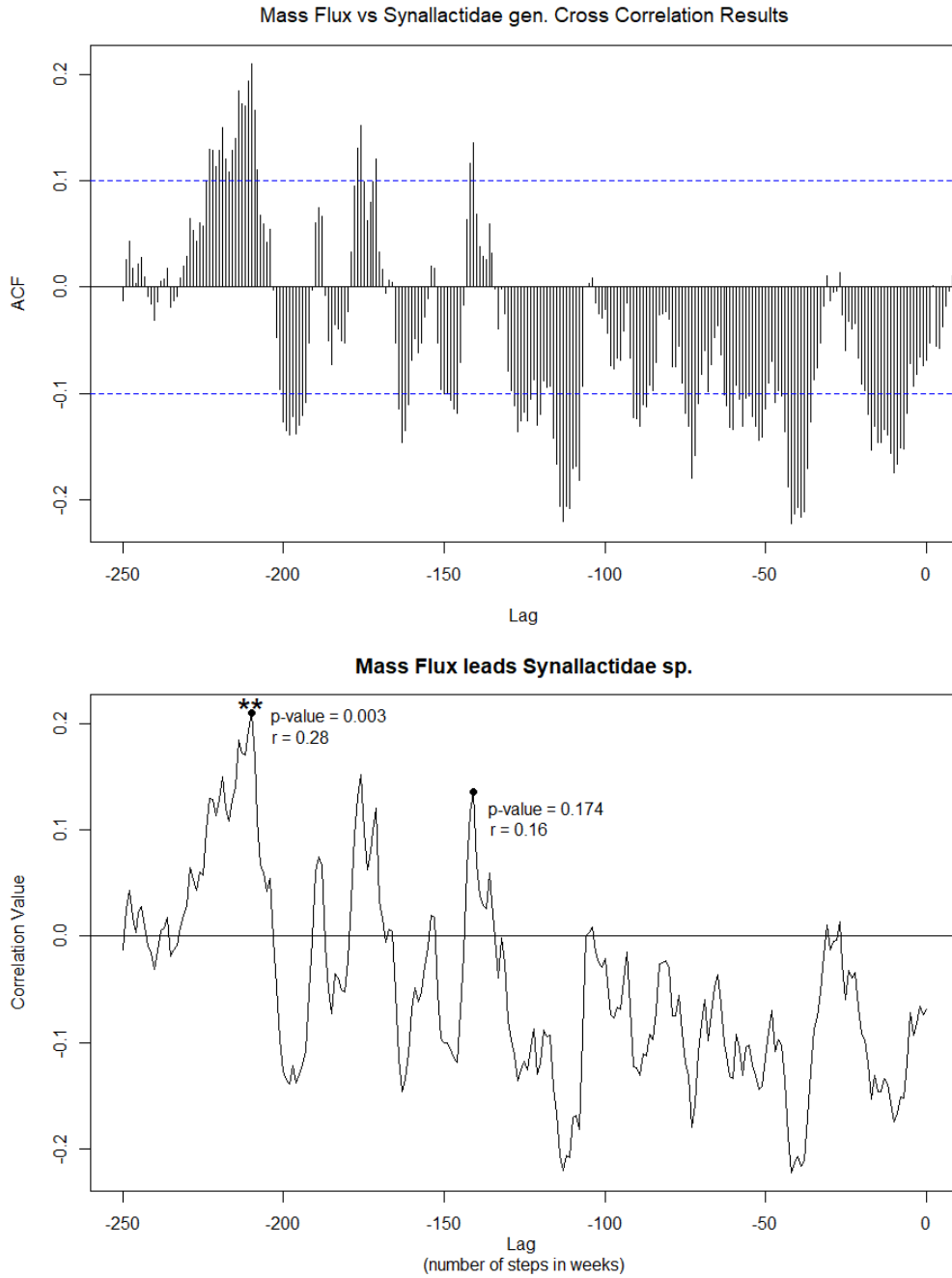


**Figure B-5.** Cross correlation results for Synallactidae gen sp. Lag in time series data. Positive correlation peaks (first and maximum) examined. Corrections for autocorrelation reflected in correlation values (r) and p-values.

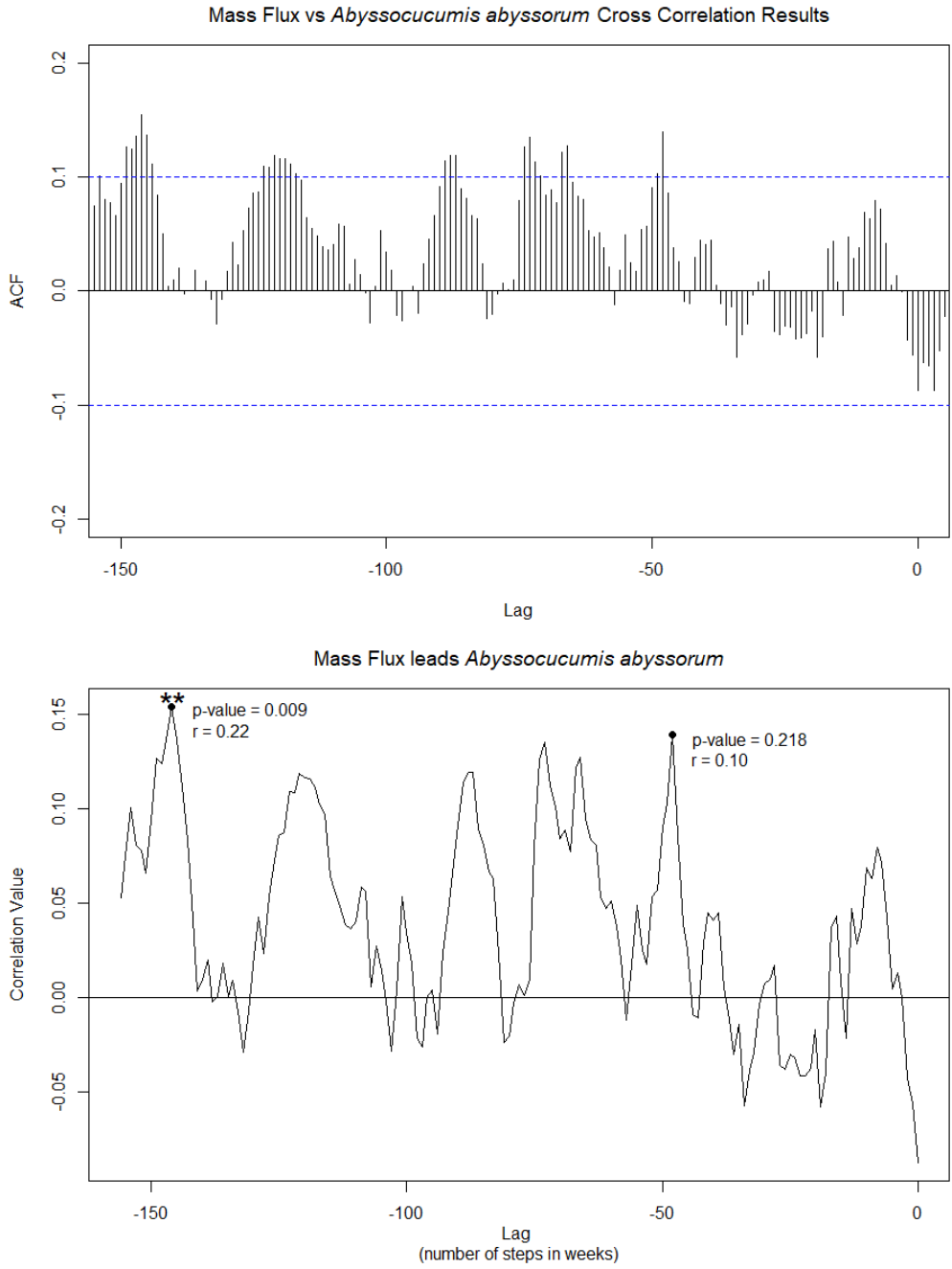


**Figure B-6.** Cross correlation results for *Abyssocucumis abyssorum*. Lag in time series data. Positive correlation peaks (first and maximum) examined. Corrections for autocorrelation reflected in correlation values (r) and p-values.

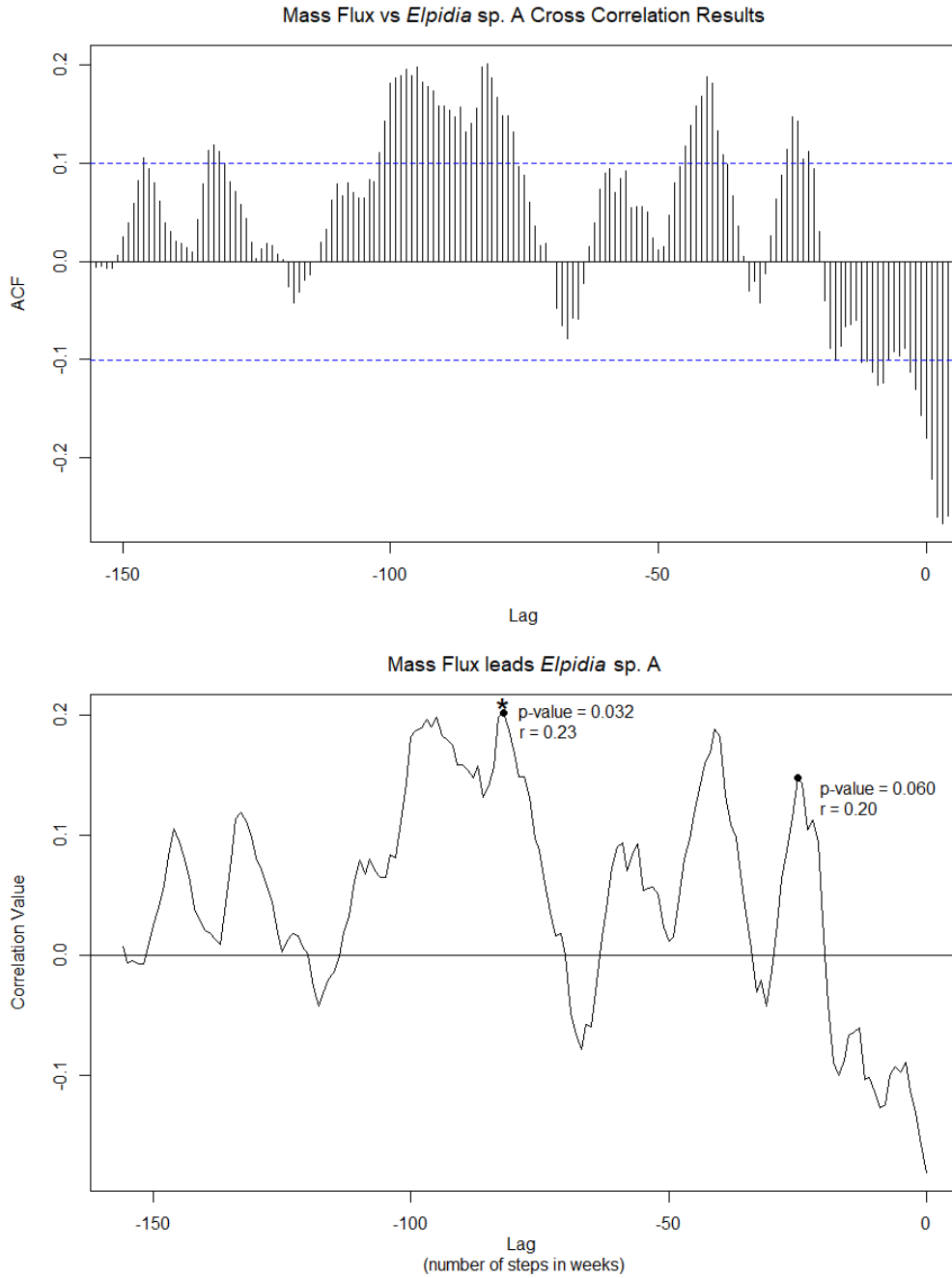


**Figure 15.** Cross correlation results for *Elpidia* sp. A. Lag in time series data. Positive correlation peaks (first and maximum) examined. Corrections for autocorrelation reflected in correlation values ( $r$ ) and  $p$ -values.

**APPENDIX C**  
**SPECIES COMPARISON BETWEEN TIME-LAPSE**  
**AND ROV TRANSECTS**

**Table C-1.** Species composition of holothurians in time-lapse and ROV imagery used in spatial distance analysis.

	High Density		Medium Density		Low Density	
	CT 62	ROV486	CT 60	ROV403	CT 68	ROV986
Total Individuals (N)	270	411	25	357	14	47
<i>Abyssocucumis abyssorum</i>	8	3	0	1	0	2
<i>Elpidia</i> sp. A	13	156	0	132	0	2
<i>Oneirophanta mutabilis</i>	0	0	0	1	1	0
<i>Paelopatides confundens</i>	0	3	0	2	0	0
<i>Peniagone gracilis</i>	0	14	0	6	0	0
<i>Peniagone papillata</i>	0	3	0	2	0	0
<i>Peniagone</i> sp.	0	1	0	7	0	2
<i>Peniagone</i> sp. 1	0	0	0	3	0	0
<i>Peniagone</i> sp. 2	0	3	0	3	0	2
<i>Peniagone</i> sp. A	220	118	22	154	2	12
<i>Peniagone vitrea</i>	3	26	1	21	0	7
<i>Psychropotes</i> spp.	0	1	0	1	0	0
<i>Scotoplanes globosa</i>	17	27	2	75	10	17
Synallactidae gen.*	0	1	0	3	1	3

## APPENDIX D

### R CODE

```
###Mass Flux vs. Population Density correlation functions

#Set up data directory
setwd("C:/ ")

#Import Ranked Data
Abund_Ranks <- read.csv(file=" ",head=TRUE, sep=",")

#Run cross correlations at a series of lags. Delete lags that are not
appropriate mechanistically. Repeat for all species. These correlation
values are to determine positive peaks in correlation, then corrected for
autocorrelation with Pypers and Peterson Method

#Max lag can be shifted for each species if necessary, data set has 382
ccfTotHoloMassFlux<- ccf(Abund_Ranks$MassFlux_Ranked,
  Abund_Ranks$Total_Holo_Ranked, plot = TRUE,
  lag.max = 156, na.action = na.pass, xlim=c(-150,0), main = "")

title("Mass Flux vs Total Holothurians Cross Correlation Results", line=0.5)

#Pull out acf values and lags
corTotHoloMassFlux=ccfTotHoloMassFlux$acf[,,1]
lagTotHoloMassFlux= ccfTotHoloMassFlux$lag[,,1]

#Put acf and lag into new data frame
resTotHoloMassFlux= data.frame(corTotHoloMassFlux,lagTotHoloMassFlux)
resTotHoloFollowsMassFlux<- resTotHoloMassFlux[1:157, ]

#Find maximum correlation and lag
resTotHoloFollowsMassFlux_max = resTotHoloMassFlux[
  which.max(resTotHoloFollowsMassFlux$corTotHoloMassFlux ),]
print(resTotHoloFollowsMassFlux_max)
resTotHoloFollowsMassFlux<- resTotHoloMassFlux[1:157, ]

#Plot correlation values with lag; insert points, p-values, and correlation
#values. Add significance when necessary calculated from the autocorrected
#values

plot(resTotHoloFollowsMassFlux$lagTotHoloMassFlux,
  resTotHoloFollowsMassFlux$corTotHoloMassFlux,
  type = "l", xlab = "Lag \n(number of steps in weeks)",
  ylab = "Correlation Value", main = "Mass Flux leads Total
  Holothurians")

#Add line at 0 to make it easier to read
abline(a=0,b=0,h=0)

#Initial positive correlation peak for total holothurians
points(-103,0.177, type = "p", pch=16)
mtext("p-value = 0.210", side=3, line=-3, adj=0.43, cex=1)
mtext("r = 0.237", side=3, line=-4, adj=0.405, cex=1)
```

```

#Maximum positive correlation peak for total holothurians
points(-149,0.2687, type = "p", pch=16)
mtext("*", side=3, line=-1.6, adj=0.09, cex=2) ##significance
mtext("p-value = 0.017", side=3, line=-1.1, adj=0.13, cex=1)
mtext("r = 0.40", side=3, line=-2.1, adj=0.12, cex=1)

#Repeat for all species with 1% or more of observations

#CCF for Peniagone sp. A
ccfPenSpAMassFlux<- ccf(Abund_Ranks$MassFlux_Ranked,
  Abund_Ranks$PenSpA_Ranked, plot = TRUE,
  lag.max = 156, na.action = na.pass, xlim=c(-150,0), main=" ")

title(expression(paste("Mass Flux vs ",italic('Peniagone '), "sp. A Cross
Correlation Results"), line=0.5))

corPenSpAMassFlux = ccfPenSpAMassFlux$acf[,,1]
lagPenSpAMassFlux= ccfPenSpAMassFlux$lag[,,1]

resPenSpAMassFlux = data.frame(corPenSpAMassFlux ,lagPenSpAMassFlux)
resPenSpAfollowsMassFlux<- resPenSpAMassFlux[1:157, ]

resPenSpAfollowsMassFlux_max = resPenSpAMassFlux[
  which.max(resPenSpAfollowsMassFlux$corPenSpAMassFlux ),]
print(resPenSpAfollowsMassFlux_max)
resPenSpAfollowsMassFlux<- resPenSpAMassFlux[1:157, ]

plot(resPenSpAfollowsMassFlux$lagPenSpAMassFlux,
  resPenSpAfollowsMassFlux$corPenSpAMassFlux,
  type = "l", xlab = "Lag \n(number of steps in weeks)",
  ylab = "Correlation Value", main = substitute(paste("Mass Flux leads
",italic('Peniagone '), "sp. A")))

abline(a=0,b=0,h=0)

#Initial positive correlation peak for Peniagone sp. A
points(-103,0.241, type = "p", pch=16)
mtext("p-value = 0.057", side=3, line=-3, adj=0.44, cex=1)
mtext("r = 0.33", side=3, line=-4, adj=0.41, cex=1)

#Maximum positive correlation peak for Peniagone sp. A
points(-149,0.29, type = "p", pch=16)
mtext("*", side=3, line=-1.6, adj=0.09, cex=2) ##significance
mtext("p-value = 0.015", side=3, line=-1.1, adj=0.14, cex=1)
mtext("r = 0.40", side=3, line=-2.1, adj=0.13, cex=1)

#CCF for Scotoplanes globosa
ccfScotoMassFlux<- ccf(Abund_Ranks$MassFlux_Ranked,
  Abund_Ranks$Scoto_Ranked, plot = TRUE,
  lag.max = 215, na.action = na.pass, xlim=c(-200,0), main=" ")

title(expression(paste("Mass Flux vs ",italic('Scotoplanes globosa'), " Cross
Correlation Results"), line=0.5))

```

```

corScotoMassFlux=ccfScotoMassFlux$acf[,,1]
corScotoMassFlux = ccfScotoMassFlux$acf[,,1]
lagScotoMassFlux= ccfScotoMassFlux$lag[,,1]

resScotoMassFlux = data.frame(corScotoMassFlux ,lagScotoMassFlux)
resScotofollowsMassFlux<- resScotoMassFlux[1:216, ]

resScotofollowsMassFlux_max = resScotoMassFlux[
  which.max(resScotofollowsMassFlux$corScotoMassFlux ),]
print(resScotofollowsMassFlux_max)
resScotofollowsMassFlux<- resScotoMassFlux[1:216, ]

plot(resScotofollowsMassFlux$lagScotoMassFlux,
      resScotofollowsMassFlux$corScotoMassFlux,
      type = "l", xlab = "Lag \n(number of steps in weeks)",
      ylab = "Correlation Value", main = substitute(paste("Mass Flux leads
",italic('Scotoplanes globosa'))))

abline(a=0,b=0,h=0)

#Initial positive correlation peak for Scotoplanes globosa
points(-176,0.112, type = "p", pch=16)
mtext("p-value = 0.053", side=3, line=-3, adj=0.26, cex=1)
mtext("r = 0.33", side=3, line=-4, adj=0.24, cex=1)

#Maximum positive correlation peak for Scotoplanes globosa
points(-203,0.164, type = "p", pch=16)
mtext("p-value = 0.471", side=3, line=-1.1, adj=0.14, cex=1)
mtext("r = 0.12", side=3, line=-2.1, adj=0.13, cex=1)

#CCF for Peniagone vitrea
ccfPenVitMassFlux<- ccf(Abund_Ranks$MassFlux_Ranked,
  Abund_Ranks$PenVit_Ranked, plot = TRUE,
  lag.max = 156, na.action = na.pass,xlim=c(-150,0), main= " ")

title(expression(paste("Mass Flux vs ",italic('Peniagone vitrea'), " Cross
Correlation Results"), line=0.5))

corPenVitMassFlux = ccfPenVitMassFlux$acf[,,1]
lagPenVitMassFlux= ccfPenVitMassFlux$lag[,,1]

resPenVitMassFlux = data.frame(corPenVitMassFlux ,lagPenVitMassFlux)
resPenVitfollowsMassFlux<- resPenVitMassFlux[1:157, ]

resPenVitfollowsMassFlux_max = resPenVitMassFlux[
  which.max(resPenVitfollowsMassFlux$corPenVitMassFlux ),]
print(resPenVitfollowsMassFlux_max)
resPenVitfollowsMassFlux<- resPenVitMassFlux[1:157, ]

plot(resPenVitfollowsMassFlux$lagPenVitMassFlux,
      resPenVitfollowsMassFlux$corPenVitMassFlux,
      type = "l", xlab = "Lag \n(number of steps in weeks)",
      ylab = "Correlation Value", main = substitute(paste("Mass Flux leads
",italic('Peniagone vitrea'))))

```

```

abline(a=0,b=0,h=0)

#Initial positive correlation peak for Peniagone vitrea
points(-53,0.153, type = "p", pch=16)
mtext("", side=3, line=-10.85, adj=0.655, cex=2)
mtext("p-value = 0.034", side=3, line=-10.4, adj=0.78, cex=1)
mtext("r = 0.21", side=3, line=-11.4, adj=0.724, cex=1)

#Maximum positive correlation peak for Peniagone vitrea
points(-100,0.318, type = "p", pch=16)
mtext("****", side=3, line=-1.6, adj=0.363, cex=2)
mtext("p-value = 0.00002", side=3, line=-1.1, adj=0.48, cex=1)
mtext("r = 0.41", side=3, line=-2.1, adj=0.435, cex=1)

#CCF for Synallactidae
ccfSynallMassFlux<- ccf(Abund_Ranks$MassFlux_Ranked,
                        Abund_Ranks$Synall_Ranked, plot = TRUE,
                        lag.max = 250, na.action = na.pass, xlim=c(-250,0), main= " ")

title(expression(paste("Mass Flux vs Synallactidae gen. Cross Correlation
                        Results")), line=0.5))

corSynallMassFlux = ccfSynallMassFlux$acf[,,1]
lagSynallMassFlux= ccfSynallMassFlux$lag[,,1]

resSynallMassFlux= data.frame(corSynallMassFlux,lagSynallMassFlux)
resSynallMassFlux = data.frame(corSynallMassFlux ,lagSynallMassFlux)
resSynallfollowsMassFlux<- resSynallMassFlux[1:251, ]

resSynallfollowsMassFlux_max = resSynallMassFlux[
  which.max(resSynallfollowsMassFlux$corSynallMassFlux ),]
print(resSynallfollowsMassFlux_max)
resSynallfollowsMassFlux<- resSynallMassFlux[1:251, ]

plot(resSynallfollowsMassFlux$lagSynallMassFlux,
     resSynallfollowsMassFlux$corSynallMassFlux,
     type = "l", xlab = "Lag \n(number of steps in weeks)",
     ylab = "Correlation Value", main = "Mass Flux leads Synallactidae sp.")

abline(a=0,b=0,h=0)

#Initial positive correlation peak for Synallactidae gen.
points(-141,0.136, type = "p", pch=16)
#mtext(" ", side=3, line=-1.6, adj=0.363, cex=2)
mtext("p-value = 0.174", side=3, line=-6, adj=0.53, cex=1)
mtext("r = 0.16", side=3, line=-7, adj=0.494, cex=1)

#Maximum positive correlation peak for Synallactidae gen.
points(-210,0.210, type = "p", pch=16)
mtext("***", side=3, line=-1.6, adj=0.175, cex=2)
mtext("p-value = 0.003", side=3, line=-1.55, adj=0.24, cex=1)
mtext("r = 0.28", side=3, line=-2.55, adj=0.224, cex=1)

#CCF for Abyssocucumis abyssorum

```

```

ccfAbyssMassFlux<- ccf(Abund_Ranks$MassFlux_Ranked,
  Abund_Ranks$Abyss_Ranked, plot = TRUE,
  lag.max = 156, na.action = na.pass, xlim=c(-150,0), main= " ", ylim=c(-
  0.2,0.2))

title(expression(paste("Mass Flux vs ",italic('Abyssocucumis abyssorum'), "
  Cross Correlation Results"), line=0.5))

corAbyssMassFlux = ccfAbyssMassFlux$acf[,,1]
lagAbyssMassFlux= ccfAbyssMassFlux$lag[,,1]

resAbyssMassFlux = data.frame(corAbyssMassFlux ,lagAbyssMassFlux)
resAbyssfollowsMassFlux<- resAbyssMassFlux[1:157, ]

resAbyssfollowsMassFlux_max = resAbyssMassFlux[
  which.max(resAbyssfollowsMassFlux$corAbyssMassFlux ),]
print(resAbyssfollowsMassFlux_max)
resAbyssfollowsMassFlux<- resAbyssMassFlux[1:157, ]

plot(resAbyssfollowsMassFlux$lagAbyssMassFlux,
  resAbyssfollowsMassFlux$corAbyssMassFlux,
  type = "l", xlab = "Lag \n(number of steps in weeks)",
  ylab = "Correlation Value", main = substitute(paste("Mass Flux leads
  ", italic('Abyssocucumis abyssorum'))))

abline(a=0,b=0,h=0)

#Initial positive correlation peak for Abyssocucumis abyssorum
points(-48,0.139, type = "p", pch=16)
#mtext(" ", side=3, line=-1.6, adj=0.363, cex=2)
mtext("p-value = 0.218", side=3, line=-3, adj=0.81, cex=1)
mtext("r = 0.10", side=3, line=-4, adj=0.75, cex=1)

#Maximum positive correlation peak for Abyssocucumis abyssorum
points(-146,0.154, type = "p", pch=16)
mtext("***", side=3, line=-1.6, adj=0.085, cex=2)
mtext("p-value = 0.009", side=3, line=-1.55, adj=0.14, cex=1)
mtext("r = 0.22", side=3, line=-2.55, adj=0.13, cex=1)

#CCF for Elpidia sp. A
ccfElpMassFlux<- ccf(Abund_Ranks$MassFlux_Ranked,
  Abund_Ranks$Elpidia_Ranked, plot = TRUE,
  lag.max = 156, na.action = na.pass, xlim=c(-150,0), main= " ")

title(expression(paste("Mass Flux vs ",italic('Elpidia '), "sp. A Cross
  Correlation Results"), line=0.5))
corElpMassFlux = ccfElpMassFlux$acf[,,1]
lagElpMassFlux= ccfElpMassFlux$lag[,,1]

resElpMassFlux = data.frame(corElpMassFlux ,lagElpMassFlux)
resElpfollowsMassFlux<- resElpMassFlux[1:157, ]

resElpfollowsMassFlux_max = resElpMassFlux[
  which.max(resElpfollowsMassFlux$corElpMassFlux ),]

```

```

print(resElpfollowsMassFlux_max)
resElpfollowsMassFlux<- resElpMassFlux[1:157, ]

plot(resElpfollowsMassFlux$lagElpMassFlux,
      resElpfollowsMassFlux$corElpMassFlux,
      type = "l", xlab = "Lag \n(number of steps in weeks)",
      ylab = "Correlation Value", main = substitute(paste("Mass Flux leads
",italic('Elpidia'), " sp. A")))

abline(a=0,b=0,h=0)

#Initial positive correlation peak for Elpidia sp. A
points(-25,0.148, type = "p", pch=16)
#mtext("*", side=3, line=-1.6, adj=0.363, cex=2)
mtext("p-value = 0.060", side=3, line=-5, adj=0.97, cex=1)
mtext("r = 0.20", side=3, line=-6, adj=0.9, cex=1)

#Maximum positive correlation peak for Elpidia sp. A
points(-82,0.202, type = "p", pch=16)
mtext("*", side=3, line=-1.6, adj=0.475, cex=2)
mtext("p-value = 0.032", side=3, line=-1.3, adj=0.57, cex=1)
mtext("r = 0.23", side=3, line=-2.3, adj=0.53, cex=1)

###Spatial Distances: Nearest Neighbor Index
##ROV transects

#Set up data directory
setwd("C:/ ")

#Nearest neighbor for ROV TRANSECT 403 (Pulse 60) all species
#Import ROV data
ROV99403 <- read.csv(file="ROV99403_Pulse60.csv",head=TRUE,sep=",")
ROV99486 <- read.csv(file="ROV99486_Pulse62.csv",head=TRUE,sep=",")
ROV99986 <- read.csv(file="ROV99986_Pulse68.csv",head=TRUE,sep=",")

#Create a window to plot coordinates of individuals NOTE: These are in
meters.
w <- as.owin(list(xrange=c(0,1),yrange=c(0,200)))

#Plot coordinates into window
holo60=ppp(ROV99403$X_distance, ROV99403$y.distance.from.beginning..m.,
           window=w, unitname=c("meters", "meters"), labels(ROV99403$ConceptName))

plot(holo60)

#Calculate nearest neighbor index for all holothurians
NN60=nnlist(holo60)
write.csv(NN60, "Puls60_NNDistances.csv")

#Determine which individual is the nearest neighbor which makes it possible
#to coordinate with measurements made in VARS
NN60Individual=nnwhich(holo60)
write.csv(NN60Individual, "Puls60_NNIndividual.csv")

```

```

#Calculate the mean nearest neighbor distances
NN_obs_min=(sum(NN60)/length(NN60))

#Calculate the expected nearest neighbor distances
NN_expected=(0.5/(sqrt(length(NN60)/(200))))

#Calculate the nearest neighbor index (NNI)
NNI60=NN_obs_min-NN_expected

#If the NNI result is:
##          < 0 then clustered
##          = 0 then random
##          > 0 then dispersed

#To determine intensity, compute Z score (a double check to above). This
#gives 95% confidence interval

#Calculate the Standard Error
SE_All= sd(NN60)/(sqrt((length(NN60)^2)/200))

#Use standard error to calculate the z score
z_score_AllHolo60= NNI60/SE_All

#If the z score result is (with 95% CI):
##          < -1.96 then clustered
##          > 1.96 then dispersed

#Initial pass at the ROV data Look at individual species to see if
#distribution patterns are different than total holothurians

#NNI for Peniagone sp. A subset
Pen_spA_60= subset(ROV99403, ConceptName=="Peniagone sp. A")

w <- as.owin(list(xrange=c(0,1),yrange=c(0,200)))

Pen_spA_60_ppp=ppp(Pen_spA_60$X_distance,
  Pen_spA_60$y.distance.from.beginning..m.,
  window=w, unitname=c("meters", "meters"), labels(ROV99403$ConceptName))

plot(Pen_spA_60_ppp)

Pen_spA_NN60=nn-dist(Pen_spA_60_ppp)

Pen_spA_NN60Individual=nnwhich(Pen_spA_60_ppp)

Pen_spA_NN_obs_min=(sum(Pen_spA_NN60)/length(Pen_spA_NN60))

Pen_spA_NN_expected=(0.5/(sqrt(length(Pen_spA_NN60)/(200))))

Pen_spA_NNI60=Pen_spA_NN_obs_min-Pen_spA_NN_expected

Pen_spA_SE= 0.26136/(sqrt((length(Pen_spA_NN60)^2)/200))

```

```

Pen_spA_z_score= Pen_spA_NNI60/Pen_spA_SE

plot(Pen_spA_60$X_distance, Pen_spA_60$y.distance.from.beginning..m.,
     ylab="meters", xlab="meters",
     main="Peniagone sp. A Distribution \nROV Transect 403", ylim=c(0,200),
     xlim=c(0,1), col= "black", pch=16)

##Repeat for other species: Elpidia sp. A; Peniagone vitrea; Scotoplanes
#globosa; Peniagone gracilis; Abyssocucumis abyssorum; Paelopatides
#confundens; Peniagone papillata; Peniagone sp. 2; Synallactidae; Peniagone
#papillata; Peniagone sp. 1; Psychropotes spp.; Oneirophanta mutabilis

##Repeat Nearest Neighbor Index with other ROV transects:
#ROV TRANSECT 486 (Pulse 62) and ROV TRANSECT 986 (Pulse 68)

###Spatial Distances: Nearest Neighbor Index
#Camera Tripod

#Import Deployment Data
#Nearest neighbor for Pulse 60 for week after ROV transect all species
Pulse60_SD <- read.csv(file="Pulse60SDCoordinates.csv",head=TRUE,sep=",")

#Create a window to plot coordinates of individuals NOTE: These are in pixels
but ROV is in meters. Pixel length will be converted post hoc
w <- as.owin(list(xrange=c(0,4350),yrange=c(800,2900)))

#Plot coordinates into window
CT60=ppp(Pulse60_SD$x, Pulse60_SD$y, window=w,
         unitname=c("pixels", "pixels"), labels(Pulse60_SD$ConceptName))

#nndist() in r is not able to pull only one timecode out, rather it compares
one time code to all other coordinates in data set; so I subset by time code
first
CT60_TTC1=subset(Pulse60_SD, TapeTimeCode=="00:00:00:13")

#Plot timecode subset into new window
CT60_TTC1_ppp=ppp(CT60_TTC1$x, CT60_TTC1$y, window=w, unitname=c("pixels",
"pixels"), labels(Pulse60_SD$ConceptName))

#Determine which individual is the nearest neighbor which makes it possible
#to coordinate with measurements made in VARS
CT60_TTC1Individual=nnwhich(CT60_TTC1_ppp)
write.csv(CT60_TTC1Individual, "Puls60_CT60_TTC1_NNIndividual.csv")

#Calculate the nearest neighbor distances in the window
NN60_TTC1=nndist(CT60_TTC1_ppp)
write.csv(NN60_TTC1, "Puls60_TTC1_NNDistances.csv")

#Calculate the mean nearest neighbor distances
NN60_TTC1_obs_min=(sum(NN60_TTC1)/length(NN60_TTC1))

#Calculate the expected nearest neighbor distances
NN60_TTC1_expected=(0.5/(sqrt(length(NN60_TTC1)/(16.91))))

```

```

#Calculate the nearest neighbor index (NNI)
NN60_TTC1_NNI60= NN60_TTC1_obs_min - NN60_TTC1_expected

#If the NNI result is:
##           < 0 then clustered
##           = 0 then random
##           > 0 then dispersed

##Repeat for all timecodes in the corresponding week to the ROV transect

CT60_TTC2=subset(Pulse60_SD, TapeTimeCode=="00:00:00:28")
CT60_TTC3=subset(Pulse60_SD, TapeTimeCode=="00:00:01:14")
CT60_TTC4=subset(Pulse60_SD, TapeTimeCode=="00:00:01:19")
CT60_TTC5=subset(Pulse60_SD, TapeTimeCode=="00:00:01:24")
CT60_TTC5=subset(Pulse60_SD, TapeTimeCode=="00:00:01:24")
CT60_TTC6=subset(Pulse60_SD, TapeTimeCode=="00:00:02:03")
CT60_TTC7=subset(Pulse60_SD, TapeTimeCode=="00:00:02:24")
CT60_TTC8=subset(Pulse60_SD, TapeTimeCode=="00:00:03:13")
CT60_TTC9=subset(Pulse60_SD, TapeTimeCode=="00:00:03:18")
CT60_TTC10=subset(Pulse60_SD, TapeTimeCode=="00:00:03:27")
CT60_TTC11=subset(Pulse60_SD, TapeTimeCode=="00:00:04:15")

#Nearest neighbor for Pulse 62 for week after ROV transect all species
Pulse62_SD <- read.csv(file="Pulse62SDCoordinates.csv",head=TRUE,sep=",")

w <- as.owin(list(xrange=c(0,4350),yrange=c(800,2900)))

CT62=ppp(Pulse62_SD$x, Pulse62_SD$y, window=w, unitname=c("pixels",
"pixels"), labels(Pulse62_SD$ConceptName))

#Repeat steps for 62 Deployment
CT62_TTC1=subset(Pulse62_SD, TapeTimeCode=="00:00:00:03")
CT62_TTC2=subset(Pulse62_SD, TapeTimeCode=="00:00:00:13")
CT62_TTC3=subset(Pulse62_SD, TapeTimeCode=="00:00:00:23")
CT62_TTC4=subset(Pulse62_SD, TapeTimeCode=="00:00:00:26")
CT62_TTC5=subset(Pulse62_SD, TapeTimeCode=="00:00:01:03")
CT62_TTC6=subset(Pulse62_SD, TapeTimeCode=="00:00:01:13")
CT62_TTC7=subset(Pulse62_SD, TapeTimeCode=="00:00:01:23")
CT62_TTC8=subset(Pulse62_SD, TapeTimeCode=="00:00:02:03")
CT62_TTC9=subset(Pulse62_SD, TapeTimeCode=="00:00:02:13")
CT62_TTC10=subset(Pulse62_SD, TapeTimeCode=="00:00:02:23")
CT62_TTC11=subset(Pulse62_SD, TapeTimeCode=="00:00:02:26")
CT62_TTC12=subset(Pulse62_SD, TapeTimeCode=="00:00:02:29")
CT62_TTC13=subset(Pulse62_SD, TapeTimeCode=="00:00:03:03")
CT62_TTC14=subset(Pulse62_SD, TapeTimeCode=="00:00:03:10")
CT62_TTC15=subset(Pulse62_SD, TapeTimeCode=="00:00:03:13")
CT62_TTC16=subset(Pulse62_SD, TapeTimeCode=="00:00:03:19")
CT62_TTC17=subset(Pulse62_SD, TapeTimeCode=="00:00:03:23")
CT62_TTC18=subset(Pulse62_SD, TapeTimeCode=="00:00:03:24")
CT62_TTC19=subset(Pulse62_SD, TapeTimeCode=="00:00:03:27")
CT62_TTC20=subset(Pulse62_SD, TapeTimeCode=="00:00:04:02")
CT62_TTC21=subset(Pulse62_SD, TapeTimeCode=="00:00:04:08")
CT62_TTC22=subset(Pulse62_SD, TapeTimeCode=="00:00:04:13")
CT62_TTC23=subset(Pulse62_SD, TapeTimeCode=="00:00:04:23")

```

```

CT62_TTC24=subset(Pulse62_SD, TapeTimeCode=="00:00:04:29")

#Nearest neighbor for Pulse 68 for week after ROV transect all species
Pulse68_SD <- read.csv(file="Pulse68SDCoordinates.csv",head=TRUE,sep=",")
head(Pulse68_SD)

w <- as.owin(list(xrange=c(750,4385),yrange=c(1100,4000)))

CT68=ppp(Pulse68_SD$x, Pulse68_SD$y, window=w, unitname=c("pixels",
"pixels"), labels(Pulse68_SD$ConceptName))

#Repeat steps for 68 Deployment
CT68_TTC1=subset(Pulse68_SD, TapeTimeCode=="00:00:51:22")
CT68_TTC2=subset(Pulse68_SD, TapeTimeCode=="00:00:52:17")
CT68_TTC3=subset(Pulse68_SD, TapeTimeCode=="00:00:52:26")
CT68_TTC4=subset(Pulse68_SD, TapeTimeCode=="00:00:53:10")
CT68_TTC5=subset(Pulse68_SD, TapeTimeCode=="00:00:53:15")
CT68_TTC6=subset(Pulse68_SD, TapeTimeCode=="00:00:54:07")
CT68_TTC7=subset(Pulse68_SD, TapeTimeCode=="00:00:54:13")

#Mann Whitney/Wilcoxon CT_ROV_Comparison

#Import data
CT_ROV_Comp= read.csv(file="CT_ROV_Comparison.csv",head=TRUE,sep=",")

#Create vectors of distances for camera tripod and ROV NN distances
P60ROV=CT_ROV_Comp$X60ROV_NNDistance
P60CT=CT_ROV_Comp$X60CT_NNDistance

#Run Mann Whitney
wilcox.test(P60ROV, P60CT)

#Repeat for other sets
P62ROV=CT_ROV_Comp$X62ROV_NNDistance
P62CT=CT_ROV_Comp$X62CT_NNDistance

wilcox.test(P62ROV, P62CT)

P68ROV=CT_ROV_Comp$X68ROV_NNDistance
P68CT=CT_ROV_Comp$X68CT_NNDistance

wilcox.test(P68ROV, P68CT)

```